A Computational Mechanistic Study of an Aza-Michael Addition and a Paal-Knorr Reaction

By

Bin Li

A thesis submitted to the Graduate Faculty of
Auburn University
in partial fulfillment of the
requirements for the Degree of
Master of Science

Auburn, Alabama
May 9, 2015

Keywords: computational chemistry, reaction mechanism, Michael addition, Paal-Knorr reaction

Approved by

Orlando Acevedo, Chair, Associate Professor of Chemistry and Biochemistry
Bradley Merner, Assistant Professor of Chemistry and Biochemistry
Konrad Patkowski, Assistant Professor of Chemistry and Biochemistry

Abstract

Computational chemistry is a rapid growing branch of chemistry that seeks to interpret chemical problems and predict chemical phenomena using mathematical approximations and computer programs. In the present work, we explored the mechanism and solvent effects of a regioselective Aza-Michael addition reaction and studied the Paal-Knorr reaction mechanism in water or choline chloride/urea deep eutectic solvent.

Chapter 1 presents a general introduction to these two areas. Chapter 2 briefly introduces the theoretical background and methodologies used in this work. Chapter 3 presents the research efforts of a joint experimental and computational study of the solvent effects for regioselective Aza-Michael addition of an amine to 5-nitronaphthalene-1,4-dione acceptor using both *ab initio* and QM/MM methods. Finally, Chapter 4 reports preliminary results of Paal-Knorr reaction mechanism under water or choline chloride/urea deep eutectic solvent.

Acknowledgment

No one can achieve accomplishments without the help of others. To all of those who supported me throughout the study of my research projects, thank you. My deepest gratitude goes first to my kind adviser, Dr. Orlando Acevedo, who guided me through my graduate education. His broad knowledge and rigorous scientific way of thinking helped me overcome difficulties along my study. His personal generosity in terms of how my career path extends is what I will never forget.

I also extend my appreciation to my lab colleagues. Symon's problem solving skills and enthusiasm towards life have been inspiring me. Billy and Caley provided me insightful instructions on my research even if they are not in the state I'm living. I'm also grateful to Kira, Nicole, Brittany and Robel who helped create and sustain such a positive atmosphere in which to do research. Most of all, I'd like to express my deepest gratitude to my family for their unceasing support and encouragement.

Table of Contents

List of Figures

List of Tables

List of Schemes

List of Abbreviations

BOSS	Biochemical and Organic Simulation Software
ChCl	Choline chloride
CC/G	ChCl with glycerol
CCSD(T)	Couple cluster single double(include triple excitations non-iteratively)
CC/U	ChCl and urea
CM1	Charge model 1
CM3	Charge model 3
CPCM	Conductor-like Polarizable Continuum Model
DESs	Deep Eutectic Solvents
DFT	Density Functional Theory
DMAD	Dimethyl azodicarboxylate
DMSO	Dimethyl sulfoxide
EWG	Electron withdrawing group
FEP	Free Energy Perturbation
GGA	Generalized Gradient Approximation
GTO	Gaussian type orbital
HBDs	Hydrogen bond donors
HMF	Hydroxymethylfurfural
ILs	Ionic liquids

LCAO-MO	Linear combination of atomic orbital molecular orbital
LDA	Local Density Approximation
MC	Monte Carlo
MC/FEP	Monte Carlo sampling and free-energy perturbation theory
MCPRO	Monte Carlo statistical mechanics simulations of peptides, proteins, and nucleic acids
MNDO	Modified neglect of diatomic overlap
NDDO	Neglect of diatomic differential overlap
MP2	Møller–Plesset perturbation: second order
NPT	isothermal-isobaric
OPLS-AA	All-Atom Optimized Potentials for Liquid Simulations
PMF	Potentials of mean force
QM/MM	Mixed quantum mechanics and molecular mechanics
r.d.s	rate determining step
RMIM	1-alkyl-3-methylimidazolium
RTILs	Room temperature ionic liquids
SCF	Self-consistent field
SDD	Semidiscrete decomposition
SMD	An universal solvation model
STO	Slater type orbital
TMS	Trimethylsilane

TS	Transition structure
TsOH	p-Toluenesulfonic acid

Chapter 1 Introduction

1.1 Solvent Effects for Regioselective Aza-Michael Addition to Enone Acceptors: An Experimental and Theoretical Study

The Michael reaction and its specific form, such as aza-Michael reaction is one of the most exploited reactions in organic chemistry.[1,2] β-Amino acid/esters/ketones/nitriles are useful intermediates for the preparation of a series of nitrogen containing bioactive natural products,[3] antibiotics[4] and chiral auxiliaries.[5] Given the significance of these biologically and synthetically interesting products, it is not surprising that a lot of methods to construct the C-N bond have been intensively studied. Although β-amino ketones can be prepared by the classical Mannich reaction,[6] it has several drawbacks, such as harsh reaction conditions and longer reaction times. Therefore, a variety of other methods have appeared in the literature for the synthesis of β-amino ketones, esters or nitriles.

One general method that has been widely used is the Michael addition of amines onto α,β-unsaturated carbonyl compounds, which is so-called "aza-Michael addition" (Scheme 1.1). The aza-Michael reaction was first reported in 1874 by Heintz, Sokoloff, and Latschinoff during their study on the reaction of ammonia with acetone or mesityloxide to form diacetone-amine.[7-9] In general, this conjugate addition of nucleophiles to unsaturated carbonyl compounds requires a basic or acidic catalyst.[10,11] However, when stoichiometric amounts of catalysts are used upon reactive substrates, several side reactions occur.[12] As a result, a wide variety of catalysts have been reported in the literature and in particular various Lewis acid-catalyzed reactions have been carried out to minimize these shortcomings.[12-14] Despite their usefulness, many of these procedures often require large amounts of reagents, prolonged reaction times and various catalysts such as lanthanide[15,16]

and precious metal complexes.[17] Use of heterogeneous catalysts for this transformation has also been developed because of their high stability, ease of handling, reusability, non-corrosive nature, long time persisting catalytic activity and environmental friendliness.[18,19] However, most heterogeneous catalytic systems sacrifice the catalysis efficiency as they dramatically reduce the mass transfer effects between reactants and catalysts.

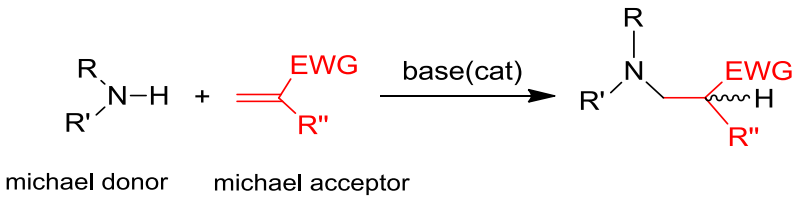

Scheme 1.1 Typical aza-Michael addition reaction

Over the last several decades, tremendous progress has been made by employing new nitrogen nucleophiles and acceptors for the aza-Michael addition reaction. Also, more efficient catalyst systems have been developed. A variety of reagents such as Pd compounds,[20] $InCl_3$,[21] and $FeCl_3 \cdot 7H_2O$[22] have been used to catalyze aza-Michael reactions under mild conditions in aqueous solution.

Water is the reaction medium used by nature in all biosynthetic pathways. It is ubiquitous in living organisms and has a lot of natural chemistry involved. However, generations of organic chemists have been trained that water should not be seriously considered as a useful reaction solvent. This was probably because of the hydrolysis effects of water with other chemicals. Water is also not miscible with the vast majority of organic compounds. However, the use of water as medium for organic synthesis has mushroomed since Sharpless and co-workers described an “on-water” approach which shows unique reactivity of organic compounds in aqueous suspensions.[23] For the cycloaddition of

dimethyl azodicarboxylate (DMAD) with quadricyclane, the "on water" method took about 10 min to enable complete reaction. Under homogeneous conditions, polar protic solvents accelerate the reaction. The reaction rates are in the following order: MeOH/H_2O (3:1)>MeOH>DMSO>CH_3CN>CH_2Cl_2>EtOAc≈toluene. This trend indicates that hydrogen bonding interactions, charge stabilization, and dipolar effects account for rate acceleration.

From the viewpoint of its use as a reaction medium, water has many favorable properties. It is non-flammable, non-toxic, stable and above all, safe, thanks to its high heat capacity[23] and unique redox stability. Furthermore, the use of water as the only reaction medium for a reaction often provides for ease of product isolation no matter whether it is "In-Water" or "On-Water" approach (Figure 1.1). In each case, the product C should not dissolve in water and should be formed in quantitative yield, consuming all of A and B such that after the filtration of C, only water should remain. Although in reality, extra processing is necessary to isolate the product and recover pure water for further use. Furthermore, the presence of buffers or catalysts are necessary for successful reactions in water. However, these are indeed big improvements over traditional methods. Therefore, it is generally accepted[24] that the combination of these desirable properties means that water is close to being the ideal green solvent.

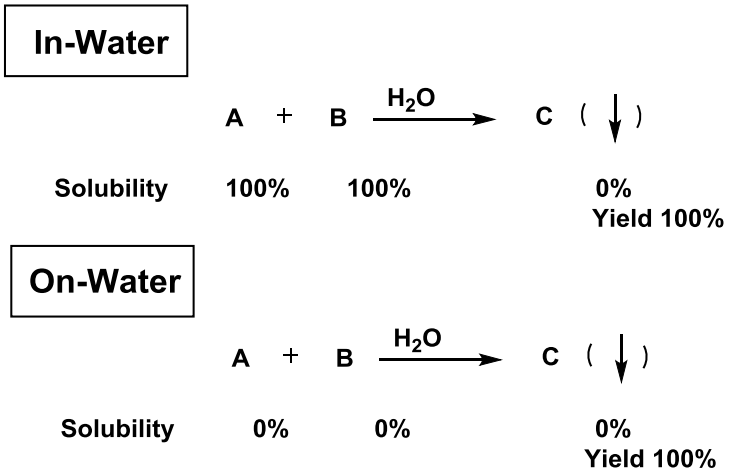

Figure 1.1 "In-water" or "on-water" approach

A number of catalytic Michael reactions using water as a solvent have been reported by a number of groups. Jorgensen and co-workers have explored the aqueous organocatalytic Michael reaction using a TMS(trimethylsilane)-prolinol organocatalyst with the reaction of β-ketoesters to α,β-unsaturated aldehydes.[25] The methodology was applied to a one-pot, five-step asymmetric synthesis of optically active cyclohexene-2-one derivatives, which are important building blocks in synthetic and medicinal chemistry (Scheme 1.2). Xiao and co-workers synthesized and applied a pyrrolidine-thiourea organocatalyst in the Michael addition reaction of ketones, such as cyclohexanone, to nitroolefins using water as the reaction medium. This catalyst could be easily tuned to obtain optimum selectivity (Scheme 1.3).[26] High yields and enantioselectivities (>99% ee) were obtained in this reaction, and there was significant functional group tolerance on the nitroolefin.

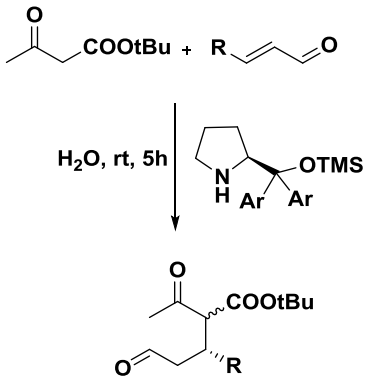

R	Solvent	Yield(%)	ee(%)
Ph	H_2O	97	94
Ph	Neat	90	94
Me	H_2O	82	84

Scheme 1.2 Aqueous organocatalytic asymmetric Michael reaction

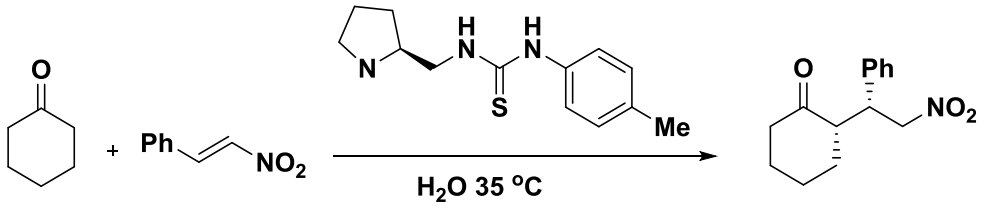

Scheme 1.3 Aqueous organocatalytic Michael addition using a pyrrolidine-thiourea organocatalyst

In addition, the "on-water" method for aza-michael addition has proved to be successful for the uncatalysed addition of aniline onto methyl acrylate using hot water (80 °C) as the solvent (Scheme 1.4). However, only 21% yield of the desired mono-alkylation product was obtained. When the more electrophilic *N*-acryloyl-2,5-dimethylpyrrole was employed, the reaction completed with 96% yield at room

temperature using water.[27] Thus, exploring "on-water" approaches for various aza-Michael reactions may be very promising area of research.

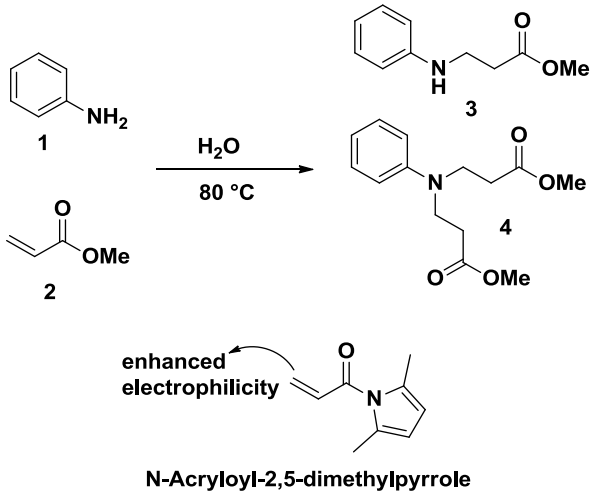

Scheme 1.4 Conjugate addition of aniline to methyl acrylate

Besides water, Ionic liquids (ILs) are often touted as green alternatives to volatile organic solvents. Ionic liquids are a unique class of solvents, defined as a material containing only ionic species (Figure 1.2). They can be fluid at temperatures as low as 204 K, have low viscosities and vapor pressures, excellent thermal and chemical stabilities, are recyclable, and tolerate impurities such as water.[28,29] Ion components can be fine-tuned through different functional groups to enhance the degree of localized structuring in the liquid phase, which distinguishes ionic liquids from molecular solvents and solutions containing dissociated ions.

Although ionic liquids are not preferable to water, their use as a medium for chemical reactions has significantly increased in recent years. Ionic liquids have been reported to be widely used in catalysis, separation processes, and organic synthesis. The first paper of the use of an IL as a catalyst in Friedel-Crafts acylation was reported in

1986.[30] In the past decade, ILs have been extensively studied in chemical reactions. This has led to an exponential growth in the number of research works that employ ILs as solvents.[28]

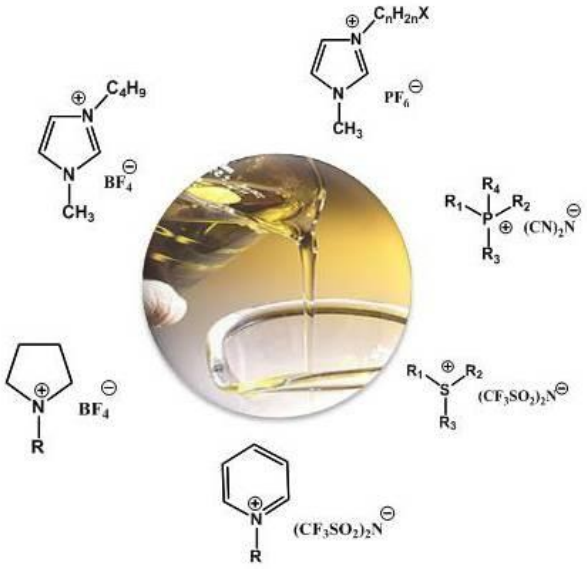

Figure 1.2 Ionic Liquids

Other than their advantages in terms of environmental impact, ILs have unique properties which make them interesting media for chemical reactions. There are a lot of cationic and anionic candidates that could form ionic liquids. This makes a wide range of physical and chemical properties possible, including volatile[31] and involatile systems, and thus the term "task-specific" ILs has been proposed.[32] This allows control over processing of the reaction. In any classical process in which the overall environmental impact and economics are of major concern, ILs have been shown to have a significant advantage over conventional solvents for homogeneously catalyzed reactions. In these cases, ILs may be used in "biphasic catalysis"[33] or the catalyst can be immobilized, allowing

extraction/distillation of the organic product and the IL/catalyst system cam be reused. Direct immobilization of ILs on a solid support has been reported.[34]

Another approach for the application of ILs application is the synthesis of active catalysts in ILs by stabilization of the metal complexes with ILs.[35] For example, in acetonitrile, palladium(II) chloride reacts with *n*-butyronitrile pyridinium chloride, $[C_3CNpy]$-Cl, **1**, leading to $[C_3CNpy]_2[PdCl_4]$, **2** (Scheme 1.5). Addition of a further equivalent of $PdCl_2$ to **2** in dichloromethane resulted in formation of $[PdCl_2(C_3CNpy)_2][PdCl_4]$, **3**, over a period of several days. The structure of these complexes has been determined from single-crystal X-ray analysis.

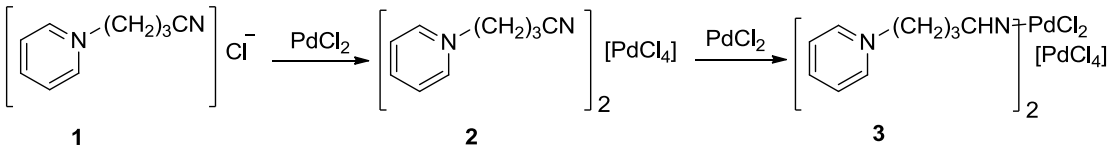

Scheme 1.5 Palladium complexes synthesis in ILs

Rather than serving as merely a solvent in classical reactions, ionic liquids have been proposed to affect the mechanism in the reaction pathway for base-induced β-elimination reactions. Utilizing mixed quantum mechanics and molecular mechanics (QM/MM) theory, Acevedo et.al. found that the presence of ionic liquids switched the reaction pathway from an E1cB-like mechanism in methanol to a pure E2 mechanism, which is consistent with experimental results.[36]

Ionic liquids have also been used in a wide range of Michael additions and related reactions. When using $Ni(acac)_2$[37,38] for the conversion of acetylacetone to methyl vinyl ketone and $Cu(OTf)_2$ for a range of addition reactions, ILs show higher rates of reaction compared with molecular solvents or under solventless conditions. Enantioselective

Michael addition reactions have also been performed in $[BF_4]^-$-based ILs using (*R*,*R*)-trans-1,2-diaminocyclohexane as the chiral auxiliary.[39] In this case enantioselectivities are up to 91% were found with good yields even when catalytic amounts of diamine were employed (Scheme 1.6).

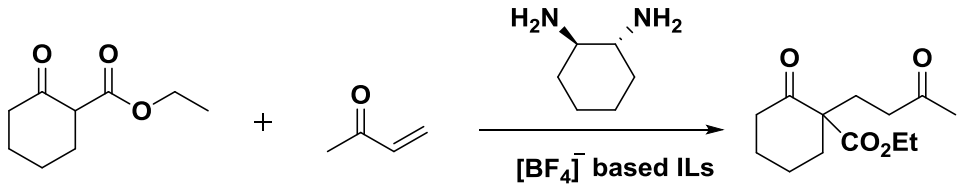

Scheme 1.6 Enantioselective Michael reaction of ethyl cyclohexanone-2-carboxylate with methyl vinyl ketone

Enantioselective Michael additions of malonates to form enones have been examined using chiral functionalized imidazolium salts with Br^-, $[BF_4]^-$, and $[PF_6]^-$ anions (Scheme 1.7) .[40] With toluene as a co-solvent, some chiral induction was achieved with yields of > 90% and enantioselectivities are between 23% and 26%. Using a dication, chiral IL reduced the ee to 10%.

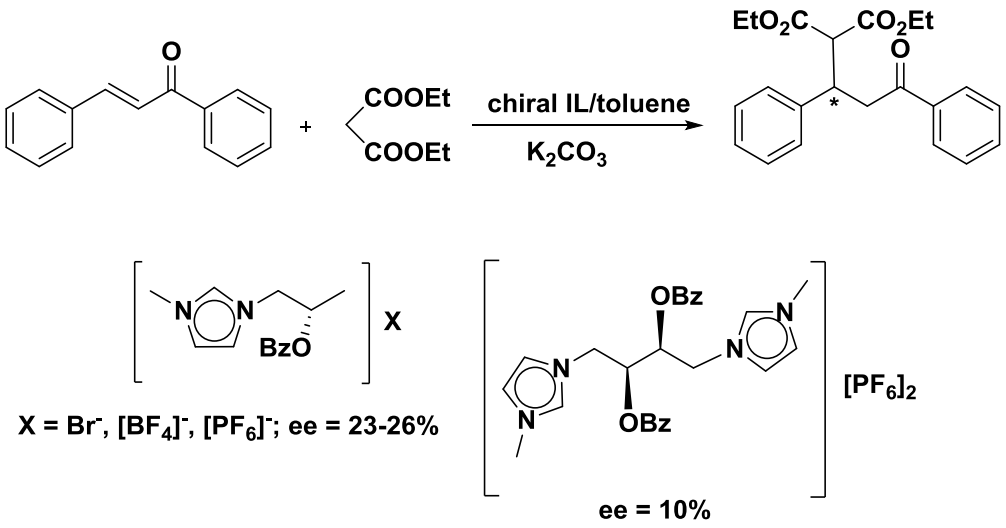

Scheme 1.7 Enantioselective Michael addition of malonates using chiral functionalized imidazolium salts

Aza-Michael addition reactions between benzylamine and ethyl acrylate have also been reported. The yields are high when using a wide range of tetraalkylammoinum halide ILs as catalysts in water.[41] In contrast, aromatic amines, such as aniline, gave poor results. This is because of the poor eletrophilicity of aniline. Furthermore, $[C_4mim][BF_4]$ has also been employed for the aza-Michael reaction of a variety of aliphatic amines and α,β-unsaturated compounds.[42] $Cu(acac)_2$ dissolved in $[C_4mim][PF_6]$ and $[C_4mim][BF_4]$ has been found to catalyze the aza-Michael reaction of amines and nitriles with α,β-unsaturated carbonyl compounds forming the corresponding β-amino carbonyl compounds and nitriles with high yields.[43]

In the present work, a computational study has been performed for the aza-Michael reaction of a primary amine to 5-nitronaphthalene-1,4-dione acceptor (Scheme 1.8). Experimental investigation shows that the major and minor products can be switched when using different solvents. Hence, the focus of the study was to rationalize the regioselectivity of this reaction.

Mixed quantum and molecular mechanical calculations utilizing Monte Carlo sampling and free-energy perturbation theory (MC/FEP) are applied to understand the solvent effects and elucidate the detailed reaction mechanism. Comparisons are made to density functional theory (DFT) calculations using an implicit continuum model to simulate conventional solvent effects.

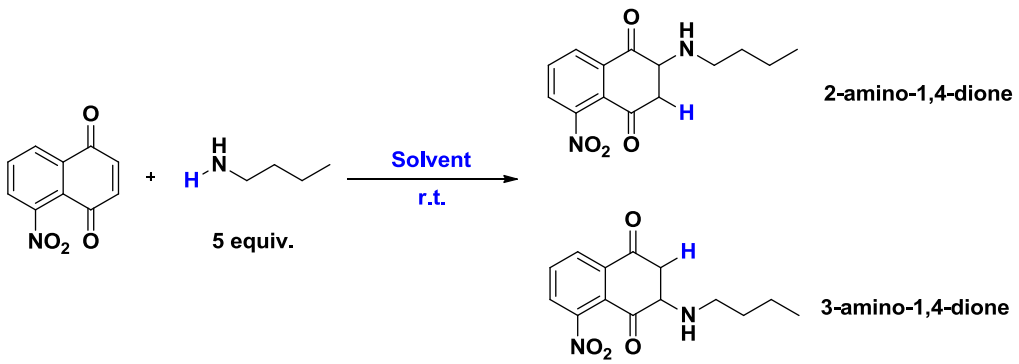

Scheme 1.8 aza-Michael addition of *n*-butylamine to 5-nitronaphthalene-1,4-dione acceptor

1.2 Paal-Knorr Reaction Mechanism Study in Deep Eutectic Solvent

Pyrroles and furans are important building blocks of various heterocyclic organic compounds, which show excellent pharmacological properties such as antibiotic,[44] antibacterial and antioxidant activities.[45] Many methods have been developed to synthesize the pyrrole or furan moiety. Among them, the Paal-Knorr synthesis of pyrroles and furans is considered to be the most powerful methodology (Scheme 1.9).

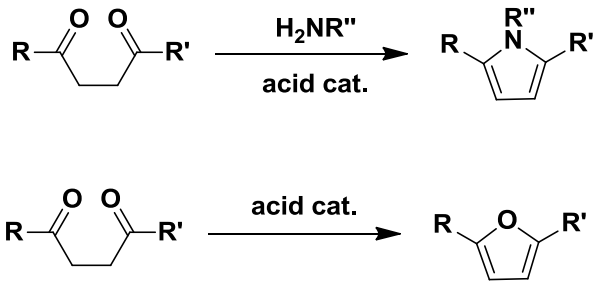

Scheme 1.9 Paal-Knorr synthesis of pyrroles and furans

Traditionally, homogeneous Brönsted or Lewis acid catalysts such as H_2SO_4, $FeCl_3$, $CoCl_2$ and $ZrOCl_2$ have been successfully employed in the Paal-Knorr synthesis. These homogeneous catalysts do have a lot of problems. The catalyst loading is usually high. Toxic and corrosive catalysts are employed and a lot of wastes are generated as the catalysts are usually not recoverable.[46,47] Large amounts of water are used to purify these products.

With respect to green chemistry, more environmentally benign methods have been developed. Heterogeneous catalysts have several advantages over homogeneous catalysts such as facile recovery and recycling, neat product separation and purification and minimum metal contamination of the products.[48] However, the catalytic efficiency of heterogeneous approaches is rather low because of mass transfer resistance.

In terms of reaction media, room temperature ionic liquids (RTILs) have been developed to replace conventional volatile solvents. In the last two decades, room temperature ionic liquids (RTILs) have attracted considerable attention especially in the fields of extraction, catalysis and electrochemistry.[28] The numbers of publications of ionic liquids as green solvents has exploded in the last two decades. Until recently, its "green affiliation" has been largely contested.[14] Most ionic liquids are toxic and they cannot bear any impurity. They are much more expensive than conventional solvents.[49] Also, synthetic procedures that employ ILs requires the use of a lot of conventional solvent for product separation and purification. A huge amount of water has to be used to neutralize the ionic liquids during the synthetic procedure.

To overcome these drawbacks of ILs, researchers have developed the deep eutectic solvents (DESs) at the beginning of this century. DESs can be made by mixing two or three cheap and safe species, which are capable of forming eutectic mixtures through hydrogen bonding interactions. Originally, eutectic mixtures were obtained by mixing quaternary ammonium salts and metal salts which form complex anions such as $Al_2Cl_7^-$ and $Zn_2Cl_5^-$, decreasing the lattice energy and then the freezing point of the mixture. In this case, the eutectic mixtures are ionic liquids. However, although it has been shown that the physico-chemical properties of DES such as surface tension, viscosity, conductivity and density are

similar to RTILs,[50] DESs cannot be considered as ILs because they can also contain a molecular component such as urea and carboxylate acids. DESs have some advantage over ionic liquids such as being easy and fast preparation, which is achieved by simply mixing halide salts with hydrogen-bond donors. Synthesis of DES is 100% atom economic. Biodegradability is much better than ionic liquids. They have low toxicity and are inexpensive. Therefore, deep eutectic solvents have the potential to replace ionic liquids in many applications such as extraction, organic synthesis and catalysis. Figure 1.3 shows some DES examples.[51]

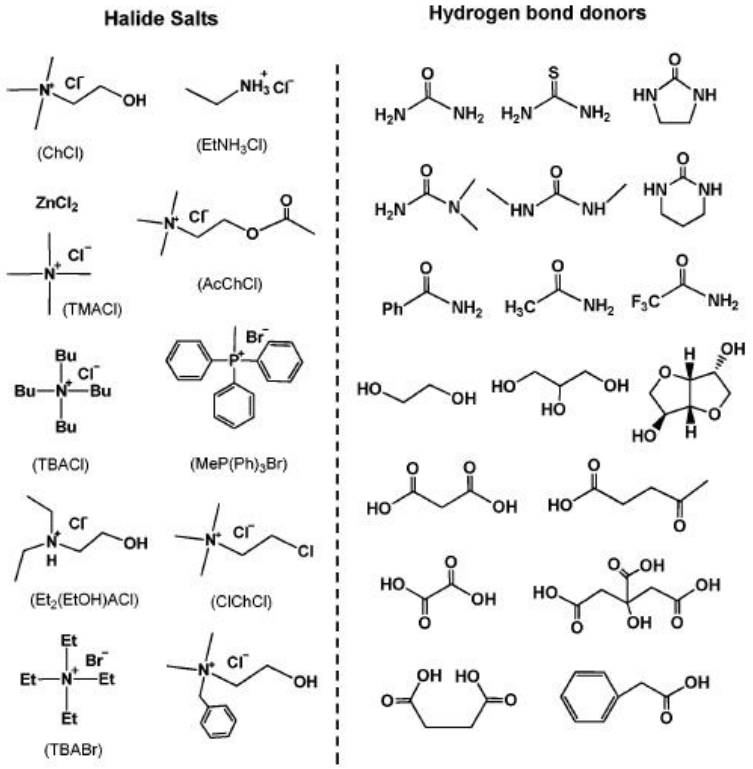

Figure 1.3 Typical structures of the halide salts and hydrogen bond donors used for DES syntheses. (Figure adapted from ref 51)

The left part of Figure 1.3 is the ionic part which can be choline chloride (ChCl), tetrabutylammonium chloride, tetramethylammonium chloride and so on. They can also be

Phosphonium salts. The right half of the figure represents various hydrogen bond donors (HBDs), such as urea, amid, glycol and carboxylic acids. Among all these combinations, choline chloride was widely used as an organic salt to produce eutectic mixtures with cheap and safe HBDs such as urea and glycerol due to their biodegradability. This is because of its biodegradability, low cost and no toxicity. Choline chloride can be either extracted from biomass or readily synthesized from fossil reserves (million metric tons) through a very high atom economical process.

Urea and glycerol are all cheap, safe and readily available HBDs. when ChCl and urea (CC/U) (Scheme 1.10) are mixed together in a molar ratio of 1:2, the freezing point of the eutectic is 12 °C, which is considerably lower than that of ChCl and urea (melting point of ChCl and urea are 302 °C and 133 °C, respectively), separately.[51] The same molar ratio of ChCl with glycerol (CC/G) (Scheme 1.11) generates an even lower freezing point. The significant depression of the freezing point comes from an interaction between the halide anion and the hydrogen bond donor component, here urea and glycerol.[52,53] (Table 1.1)

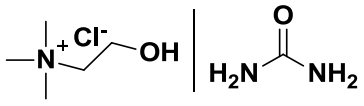

Scheme 1.10 Choline Chloride/Urea

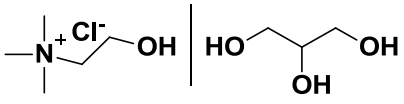

Scheme 1.11 Choline Chloride/Glycerol

Table 1.1 Physico-chemical properties of CC/U and CC/G[52]

Organic Salts	HBD	Salt : HBD molar ratio	T_f/˚C	Density (ρ, g cm^{-3})(25 ˚C)	Viscosities (cP)(25 ˚C)	Conductivity (K, Ms cm $^{-1}$)
ChCl	Urea	1 : 2	12	1.25	750	0.199 (40 ˚C)
ChCl	Glycerol	1 : 2	-40	1.18	376	1.05 (20 ˚C)

Preliminary ecological evaluation of various solvent systems has been accomplished to provide with more details about those most commonly used solvents in terms of environmental effect. Figure 1.4 was adapted from König's work which was published in 2009.[54] The solvent systems studied include water, dimethylformamide, DMSO, acetone/DMSO, AcOEt/ChCl/citric acid, [C_2mim]Cl, [C_4mim]Cl. Both ionic liquids and choline chloride/citric acid have low mobility due to their negligible vapor pressure. Chloride/citric acid has been shown to have low toxicity, whereas there is no sufficient data for ionic liquids to assess their toxicological risks to humans and other organisms. For the assessment of biodegradation, MSDS data indicates that ionic liquids are not readily biodegradable. Their persistence in environment is classified as "medium-high". It has been reported that ILs with short alkyl (<7) and short functionalized side chains are not biodegradable, while those consisting of imidazolium and pyridinium cations with octyl chains are biodegradable.[55] In conclusion, choline/chloride is preferable as reaction media over ionic liquids from the green perspective.

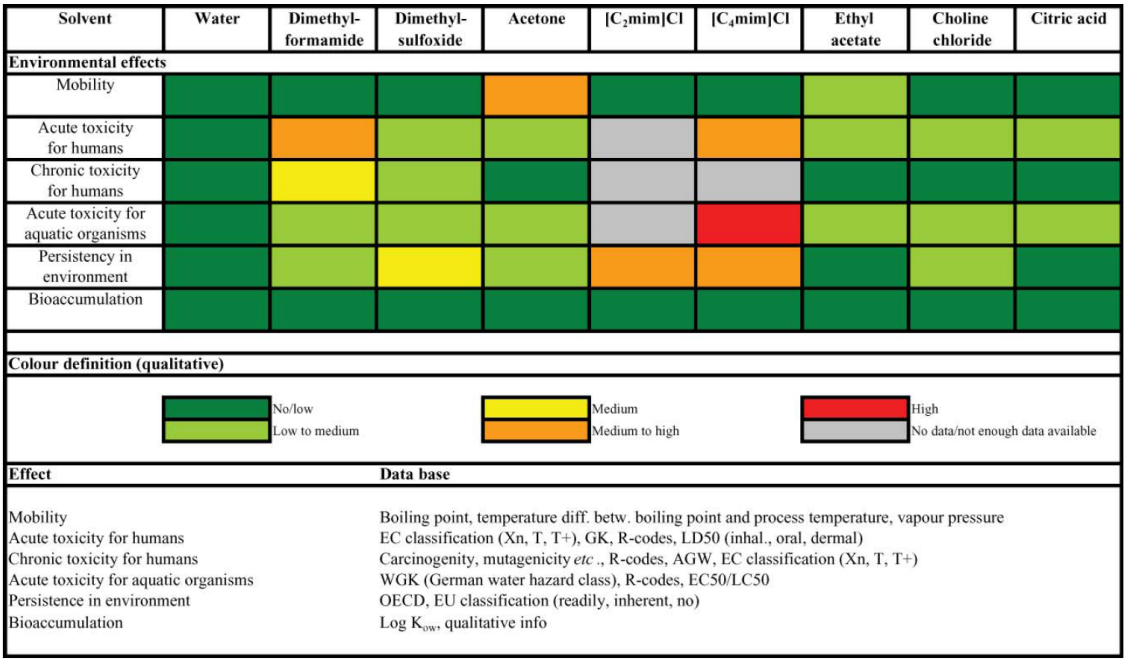

Figure 1.4 Ecological evaluation of various solvent systems (Figure adapted from ref 54)

DESs have been used as solvent in various acid or base-catalyzed reactions. König and co-workers reported the dehydration of *d*-fructose, *d*-glucose and other di- and oligosaccharides into HMF using acid catalysts in ChCl/Urea deep eutectic solvents (Scheme 1.12).[54] The catalysts used include $CrCl_2$, $ZnCl_2$, $FeCl_3$, $FeCl_2$, Amberlyst-15, $CrCl_3$, pTsOH, $Sc(OTf)_3$, Montmorillonite. The catalyst loadings for homogenous catalyst are 10 mol% and 5 wt% based on sugar. Choline chloride was found to be the most suitable additive because it is chemically inactive under the reaction conditions. When it combines with fructose at molar ratio 6:4, the melting region of the mixture is 79-82 ˚C.

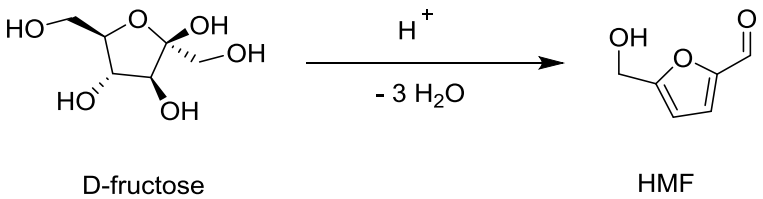

Scheme 1.12 Acid-catalyzed dehydration of d-fructose to HMF

DESs have also been used as solvent for base-catalyzed reaction which shows great recyclability and remarkable efficiency of energy utilization. Shankarling and co-workers synthesized cinnamic acid derivatives using the Perkin reaction in choline chloride/urea (1:2) (Scheme 1.13).[56] All reactions are carried out at 30 °C, and after the reaction was complete, the recovered DES can be reused for three further runs without significant decrease in product yields. NMR analysis indicated that the structure of DES has not changed during the process of the reaction. This DES-assisted method can save more than 62% of energy utilized for conventional methods.

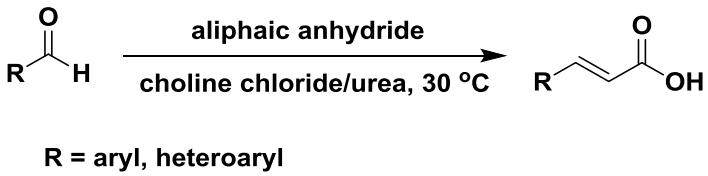

Scheme 1.13 Base-catalyzed synthesis of cinnamic acid in choline chloride/urea mixture

In terms of transition metal catalyzed reactions, DESs have been used to replace traditional solvents in catalytic C-C bond coupling reactions. Take the palladium-catalyzed Suzuki coupling of boronic acid with aryl bromides in various carbohydrates (fructose, maltose, et al.)/urea (or dimethylurea)/salts (NaCl or NH_4Cl) DESs (Scheme 1.14) for example,[57] the coupling products were obtained with up to 98% yield.

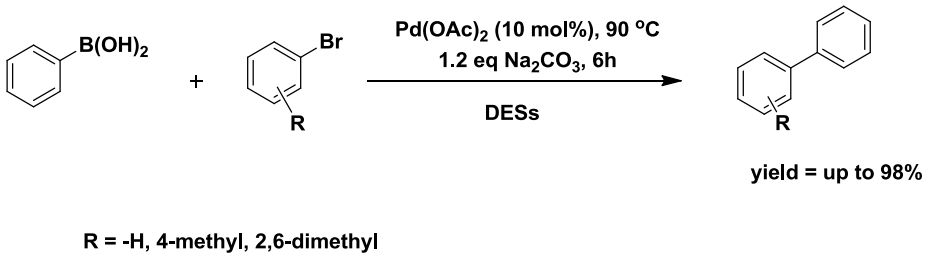

Scheme 1.14 Palladium catalyzed Suzuki coupling in DESs

For the Paal-Knorr synthesis of pyrroles and furans, Handy et. al. used choline chloride/urea to substitute for acid catalyst and obtained good to excellent yield of pyrroles with respect to the amine used (Scheme 1.15, Table 1.2) For the side reaction in which oxygen directly attacks the sp^2 hybridized carbon, the furan product was obtained with about 5 to 10% yield.[58]

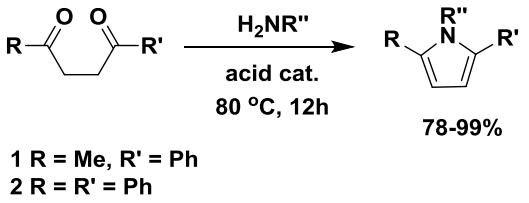

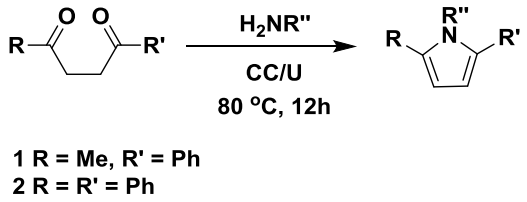

Scheme 1.15 Paal-Knorr synthesis of pyrroles in CC/U

Table 1.2 Paal-Knorr synthesis of pyrroles using different amines

Entry	Dione	Amine	Yield[a]
1	1	Benzyl	94
2	1	Hexyl	91
3[b]	1	Phenyl	88
4[b]	2	Benzyl	87
5[b]	2	Hexyl	89
6[b]	2	Phenyl	82

[a] Isolated yields.
[b] These reactions were allowed to run for 24 h instead of 12h.

Surprisingly, when amine was removed, furan was obtained almost exclusively, regardless of how the R and R' groups look like, although a prolonged time was required for the phenyl substituted reactant (Scheme 1.16). Handy proposed that the urea could activate the carbonyl group through a N-H-O hydrogen bonding interaction (Figure 1.5),

which increases the electrophilicity of the sp^2 carbon. In the present study, we focused on the furan synthesis to predict the mechanism.

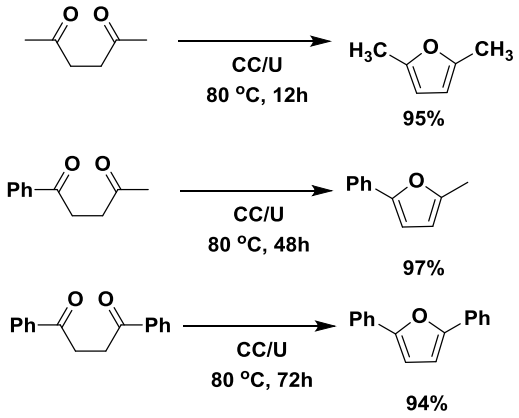

Scheme 1.16 Paal-Knorr synthesis of furan

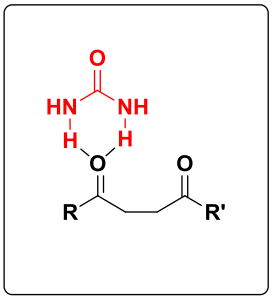

Figure 1.5 Urea as an organocatalyst

Although the reaction has been known for more than one century, the mechanism is still heavily debated. The generally accepted pathway is cyclization of the monoenol (Scheme 1.17). However, there is little experimental evidence could support this pathway. The motivation of this mechanism study work is that, the author found *d*, *l* and *meso* diastereomers of 2,3-disubstituted-1,4-diketones show different reactivity for the Paal-Knorr synthesis of pyrrole.[59,60]

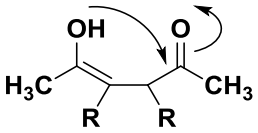

Scheme 1.17 Enol intermediate in the Paal-Knorr reaction

To test if this is also the same case for furan synthesis, Amarnath performed several kinetic experiments using the *d, l* and *meso*-diastereomers of 2,3-disubstituted-1,4-diketones (Scheme 1.18).[61] This new experimental evidence gives us a better understanding of the mechanism for Paal-Knorr synthesis of furans. Different substituent groups at the 2, 3-positions, such as methyl, ethyl, phenyl, isopropyl were employed to study the stereochemical aspects.

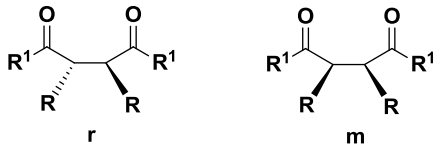

	R^1	R
1	CH_3	CH_3
2	CH_3	C_2H_5
3	CH_3	$CH(CH_3)_2$
4	C_6H_5	CH_3
5	C_6H_5	C_2H_5

Scheme 1.18 *d, l* and *meso* diastereomers of 2,3-disubstituted-1,4-diketones

Surprisingly, in water, the *meso* isomer of 3,4-dimethyl-2,5 hexanedione (**1m**) was found to cyclize to furan faster than the racemic mixture **1r**. However, the order of reactivity was reversed when the substituents at the 3- and 4-positions of the 1,4-dione were ethyl groups. In nonaqueous solvents, the kinetic trend is similar to that in water.

The application of aliphatic diones was next extended to the diastereomers of the aromatic diketones. The cyclization of these diones was carried out in a mixture of methanol and $CHCl_3$ catalyzed by HCl (Scheme 1.19). The same rate trend was found as for the aliphatic diones.

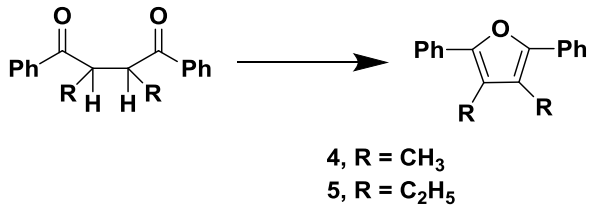

Scheme 1.19 Furan formation from 2, 3-dimethyl- and 2,3-diethyl-1,4-diphenyl-1,4-butanediones

During the reaction, each of the two carbons between the carbonyl groups loses a hydrogen atom. In order to determine whether the C-H bond cleavage occurred before or after the rate-limiting step, the *racemic* and *meso* isomers of 2, 3-dideuterio-2,3-dimethyl-1,4-butanediones(d^2-**4r** and d^2-**4m**) were prepared by deuterium exchange (Scheme 1.20).

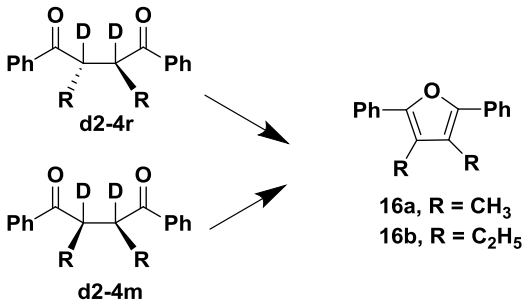

Scheme 1.20 Formation of furan from racemic and *meso* isomers of 2,3-dideuterio-2,3-dimethyl-1,4-butanediones (d^2-4r and d^2-4m)

Deuterium labeling was found to lower the rate of cyclization by a factor of 8 for **4r** and by a factor of 6.53 for **4m**. This compares well with the value generally attributed to a primary kinetic isotope effect of acid-catalyzed C-H bond cleavage during enolization

of acetone. The value for acetone is 7.9. Therefore, C-H cleavage does not occur after the rate determining step. In addition, unchanged d^2-**4r** and d^2-**4m** retained their labels, suggesting that under these conditions cyclization took place more rapidly than enolization.

There are generally four controversial mechanistic pathways used to describe the Paal-Knorr reaction (Scheme 1.21). Pathway a is the enol intermediate structure with a methylene group. Pathway b is the generally accepted mechanism, the slowest step could either be the enolization of **10b** or the ring closure to dihydrofuran. In pathway c, enolization and cyclization occur simultaneously. In pathway D, cyclization goes first then follows proton transfer. Dehydration of intermediate **12** (or **14**) to the product can be expected to be rapid and irreversible, due to aromatization of furan.

Pathway a requires cyclization to take place more slowly than enolization, but it had already been demonstrated that cyclization took place more rapidly than enolization in the previous discussion. So pathway A was denied.

In pathway b, suppose enolization is the rate determining step (r.d.s), however, the rate of acid-catalyzed enolization is known to be not sensitive to the ketone structure. This approach is not reasonable. Suppose cyclization is the rate determining step, no reactivity difference should be expected for *d, l* and *meso* isomers. As the left half part of **11b** is a planar structure, they would be expected to react at the same rate. This cannot explain the experimental results that *d, l* and *meso* isomers have different reaction rates and thus denies the possibility that cyclization in **11b** is the rate determining step.

In Pathway d, the nucleophilic attack of one carbonyl oxygen to the other protonated carbonyl resulted in an oxonium intermediate, then followed by rapid proton removal from **13**. If loss of hydrogen occurs after the rate limiting step, deuterium

substitution at the 3- and 4-positions of 3,4-dimethyl-2,5-hexanedione may be expected to cause only a slight variation in the rate of cyclization. But during the cyclization, deuterium causes a large

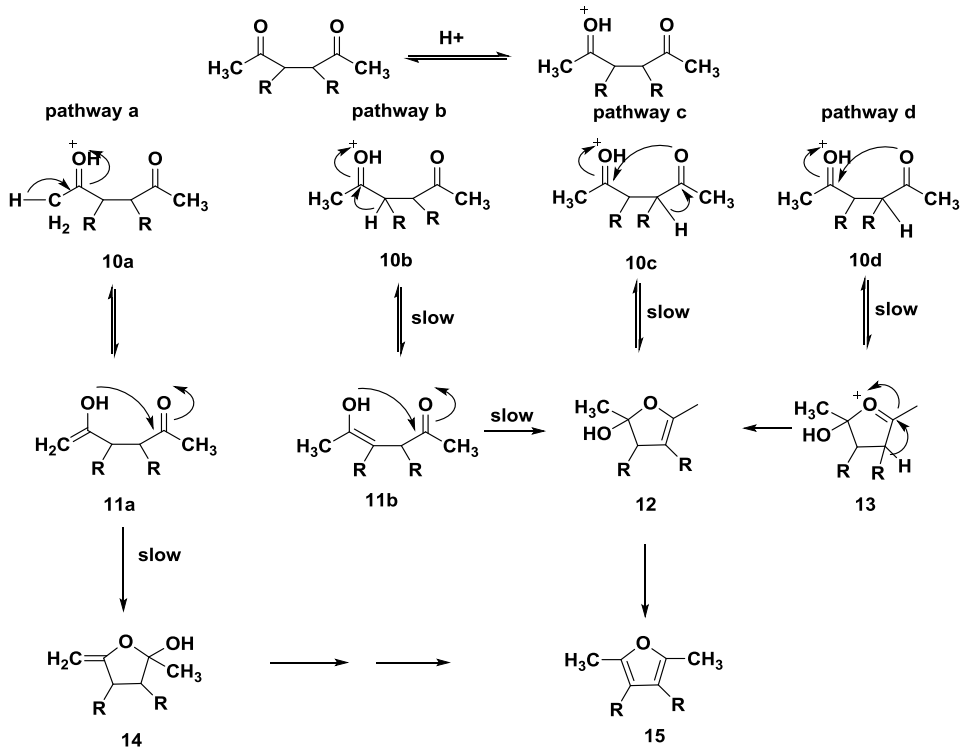

Scheme 1.21 Four proposed mechanism pathways for Paal-Knorr reaction

decrease in reaction rate (8.0 and 6.5). This indicates a primary isotope effect,[62] requiring that the carbon-hydrogen bond be broken during or before the rate limiting step. This does not support pathway D.

The concerted cyclization to ring closure product **12** (pathway c) seems to explain the kinetic results better than pathways b and d. The difference in reactivity between the diastereomers of a 1,4-diketone can be explained by looking at the Newman projections across C-3 and C-4 atoms of the protonated dione **10c** (Scheme 1.22).

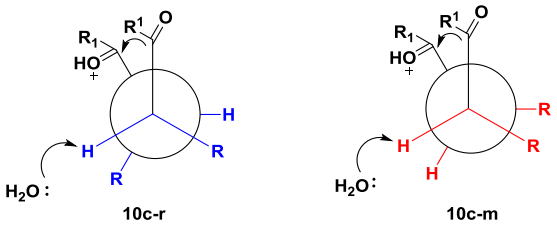

Scheme 1.22 Newman projections across C-3 and C-4 atoms of the protonated dione 10c.

Obviously, it is less hindered for the base, water in this case, to attack H in **10c-m** than to attack H in **10c-r**. Also, the *meso* isomer is an unfavorable eclipsed structure when the cyclization step takes place. But when R is methyl, its eclipsed effect is less important compared to the much favored base access to proton. Thus, dimethyl substituted *meso* isomer performs the ring closing step faster than racemic isomers. As the substitute groups become larger and larger, the unfavorable eclipsed effect of **10c-m** becomes more and more important and thus, reduces the overall reaction rates. This fits to the experimental observation that $k_{d,l}/k_{meso}$ ratio of diethyl and diisopropyl are 2.1 and 6.2, respectively.

Based on this mechanism study and experimental results, we performed our Paal-Knorr reaction mechanism of forming furan using both quantum mechanical and mixed quantum and molecular mechanical methods. The above proposed reaction pathway was studied in conventional solvents and in choline chloride/urea deep eutectic solvent.

Chapter 2 Methods

Computational chemistry is a rapidly growing branch of chemistry that uses mathematical approximations and equations as well as computational software to get information about chemical problems. It calculates the structures and properties of molecules, simulates reactions in order to interpret and predict chemical phenomena. Computational quantum chemistry focuses on equations and approximations relative to quantum mechanics. Specifically, it is to solve the Schrödinger equation for specific molecular systems. *Ab initio* quantum chemistry only uses methods that don't incorporate experimental data or empirical parameters. "*Ab initio*" is widely used to mean "from first principles."

There are many properties that can be calculated by computational chemistry. We are only listing a few here:

1) Equilibrium and transition structures
2) Reaction rates
3) Thermochemical data such as bond dissociation energy and enthalpies of formation
4) Polarizabilities and dipole moments
5) NMR, IR, Raman and UV spectra

2.1 *Ab initio* Quantum Chemistry

2.1.1 Schrödinger equation

The starting point of any quantum mechanics discussion is the Schrödinger equation, which describes the system's wavefunction that is evolving with time. The time-dependent form of the Schrödinger equation for single particle is

$$\left\{-\frac{\hbar}{2m}\left(\frac{\partial^2}{\partial x^2}+\frac{\partial^2}{\partial y^2}+\frac{\partial^2}{\partial z^2}\right)+V\right\}\psi(r,t)=i\hbar\frac{\partial\psi(r,t)}{\partial t} \qquad \textbf{(2.1.1)}$$

ħ is Planck's constant divided by 2π and i is the square root of -1, m is the mass of a single particle, x, y, z are denoted as spatial coordinate. Ψ is the wavefunction of the system and characterizes the particle's position and momenta.[63]

When the external potential does not change with time, the wavefunction can be written as the product of a spatial function and a time function: $\Psi(\mathrm{r}, t) = \Psi(\mathrm{r})T(t)$. We are only interested in solving this time-independent Schrödinger equation:

$$\left\{-\frac{\hbar}{2m}\nabla^2 + V\right\}\psi(r) = E\psi(r) \qquad \textbf{(2.1.2)}$$

The eigenvalue E is the energy of the particle and $\nabla^2 = \frac{\partial^2}{\partial x^2} + \frac{\partial^2}{\partial y^2} + \frac{\partial^2}{\partial z^2}$. It is simple and straightforward to abbreviate the Schrödinger equation to a multinuclear, multielectron system.

$$\hat{H}\psi = E\psi \qquad \textbf{(2. 1. 3)}$$

Where $\hat{H}$ is the Hamiltonian operator (or simply the Hamiltonian), which in its complete form

$$\hat{H} = -\frac{\hbar^2}{2}\sum_{\alpha}\frac{1}{m_\alpha}\nabla_\alpha^2 - \frac{\hbar^2}{2m_e}\sum_i \nabla_i^2 + \sum_\alpha\sum_{\alpha>\beta}\frac{Z_\alpha Z_\beta e'^2}{r_{\alpha\beta}} - \sum_\alpha\sum_i\frac{Z_\alpha e'^2}{r_{i\alpha}} + \sum_j\sum_{i>j}\frac{e'^2}{r_{ij}} \qquad \textbf{(2. 1. 4)}$$

m_α is the mass of nucleus α, m_e is the mass of an electron, Z is the nuclear charge, $r_{\alpha\beta}$ is the distance between nuclei α and β, r_{ij} is the distance between electrons i and j and $r_{i\alpha}$ is the distance between electron i and nucleus α. e′ is the electron charge. The left most part of this equation expresses the nucleous kinetic energy, then electron kinetic energy, nuclear-nuclear repulsion, nuclear-electron attraction and the right most is the electron-electron repulsion.[63] All *ab initio* calculations of energy in this research are based on this time-independent form of Schrödinger equation.

The many-electron Schrödinger equation, however, can't be solved exactly, even for the two-electron hydrogen molecule. Many practical methods have been made to approximately solve this problem.

2.1.2 Born-Oppenheimer Approximation

The many electron wave-function is a function of nuclear and electron coordinates: $\psi(R,r)$, R is nuclear coordinates and r is electron coordinates. The motions of nuclei and electrons are coupled with each other. However, the mass of a proton is approximately two thousand times the mass of an electron. Hence, nuclei are almost stationary compared to electrons. The nuclei appear fixed compared to the electrons. This is called "the Born-Oppenheimer approximation".[64] This approximation reflects a system with fixed nuclei and dynamic electrons. Hence, we can separate the full wave-function into a nuclear function ψ_N and an electron function ψ_{el} but still maintain a high degree of accuracy:

$$\boldsymbol{\psi = \psi_N \psi_{el}} \tag{2.1.5}$$

Now, the electronic part of the Schrödinger equation can be solved separately.

$$\hat{H}_{el}\boldsymbol{\psi_{el} = E_{el}\psi_{el}} \tag{2.1.6}$$

$$\hat{H}_{el} = -\frac{\hbar^2}{2m_e}\sum_i \nabla_i^2 - \sum_\alpha \sum_i \frac{Z_\alpha e'^2}{r_{i\alpha}} + \sum_j \sum_{i>j} \frac{e'^2}{r_{ij}} \tag{2.1.7}$$

If the electron part can be separated from the nuclear motions, then the electronic structure can be solved for any set of nuclear positions.

According to Born-Oppenheimer approximation, nuclei are relatively stationary in a molecular system. The system has zero nuclear kinetic energy. Hence, the total energy E for the system can be expressed as Equation 2.1.8:

$$\mathbf{E} = \mathbf{E_{el}} + \sum_{\alpha} \sum_{\alpha>\beta} \frac{\mathbf{Z_\alpha Z_\beta e'^2}}{\mathbf{r_{\alpha\beta}}} \quad \textbf{(2.1.8)}$$

2.1.3 Slater determinant

So how do we solve electronic Schrödinger equation? We know how to solve the electronic part for the hydrogen atom, which has only one electron. The electron-electron interaction part in equation 2.1.8 is still intractable for systems involving more than one electron. It might be plausible to think that electrons move independently of each other. If that was true, then the Hamiltonian can be separated for different electrons. The total electron wavefunction ψ describing the motions of M electrons would be the product of M hydrogen atom wavefunction (Equation 2.1.9), which is known as Hartree Product.

$$\boldsymbol{\psi_{HP}}(\mathbf{r_1}, \mathbf{r_2}, \ldots \mathbf{r_M}) = \boldsymbol{\varphi_1}(\mathbf{r_1})\boldsymbol{\varphi_2}(\mathbf{r_2}) \ldots \boldsymbol{\varphi_M}(\mathbf{r_M}) \quad \textbf{(2.1.9)}$$

For the simplest two-electron system, molecular hydrogen, the Hartree product would be

$$\boldsymbol{\psi} = \boldsymbol{\varphi_\sigma}(\mathbf{1})\boldsymbol{\alpha}(\mathbf{1})\boldsymbol{\varphi_\sigma}(\mathbf{2})\boldsymbol{\beta}(\mathbf{2}) \quad \textbf{(2.1.10)}$$

α, β are spin-functions (spin-up, spin-down), φ_σ is spatial function (molecular orbital), $\varphi_\sigma\alpha, \varphi_\sigma\beta$ are called spin-orbitals.

It seems to be pretty convenient to solve electronic wavefunction using Hartree product. The total energy of the molecule is just the sum of individual single-electron spin orbitals. However, this function form fails to meet the antisymmetric principle (Pauli Principle): if two electrons interchange space-spin coordinates with each other, the new wavefunction must have the opposite sign of the former wavefunction.[65] Also the Hartree product fails to produce an accurate energy as it assumes electrons do not have interactions with one another. So the Hartree product is very far from being the ideal approximation.

After the Born-Oppenheimer Approximation, the next important approximation employed is the expansion of the total electronic wavefunction ψ into a linear combination of Slater determinants (Equation 2.1.11 and 2.1.12).[64] N is the number of electrons and the factor $\frac{1}{\sqrt{N!}}$ ensures that the wavefunction is normalized. A Slater determinant can be regarded as molecular orbitals representative of the electronic configuration.

$$\boldsymbol{\psi_{el} = \sum_i d_i \phi_i = d_0\phi_0 + d_1\phi_1 + d_2\phi_2 + \cdots} \quad \textbf{(2.1.11)}$$

$$\Phi_0 = \frac{1}{\sqrt{N!}} \begin{vmatrix} \phi_1\alpha(1) & \phi_1\beta(1) & \phi_2\alpha(1)\ldots & \phi_M\beta(1) \\ \phi_1\alpha(2) & \phi_1\beta(2) & \phi_2\alpha(2)\ldots & \phi_M\beta(2) \\ \cdots & \cdots & \cdots & \cdots \\ \phi_1\alpha(N) & \phi_1\beta(N) & \phi_2\alpha(N)\ldots & \phi_M\beta(N) \end{vmatrix} \quad \textbf{(2.1.12)}$$

Take Be for example, the ground-state electron configuration of Be is $1s^2 2s^2$. This would be φ_0. φ_1 would be $1s^2 2s^1 2p^1$. If we have a complete set of φ_i, this would be the exact solution to the Schrödinger equation. Obviously, this is not feasible.

2.1.4 Basis set approximation

Slater determinants are based on molecular orbitals. What will be the proper solution to these orbitals? Molecules are made up of atoms. It is feasible to expect that molecular solutions should be made up of atomic solutions. The molecular orbitals in Slater determinant can be expressed as a linear combination of atomic orbitals (Equation 2.1.13).

$$\boldsymbol{\phi_i = \sum_{k=1}^{M} c_{ki}\, \chi_k} \quad \textbf{(2.1.13)}$$

Where M is the total number of atomic orbitals, c_{ki} is the molecular orbital coefficients, the basis function χ_k are atomic orbital functions that mimic solutions of H-

atom. This expansion is referred to as the linear combination of atomic orbital molecular orbital (LCAO-MO).

The form of basis functions must describe orbitals accurately. H-atom orbitals are good starting point, but real orbitals' size is not fixed and they are distorted by polarization effect. They not only have non-valence electrons but also valence electrons. At least, a function that describes H-atom orbital is a good approach to start off. The radial dependence of the hydrogen atom are Slater type functions (Equation 2.1.14)

$$\boldsymbol{\chi_{\alpha,n,l,m}(r,\theta,\varphi) = NY_{l,m}(\theta,\varphi)r^{n-1}e^{-\alpha r}} \qquad \textbf{(2.1.14)}$$

Where n is the principal quantum number, l is the azimuthal quantum number, m is the magnetic quantum number, r, θ, φ are spherical polar coordinates.[63]

Although Slater type orbitals could represent the shape of atomic orbitals very well, most calculations use Gaussian type orbitals because they comprise a polynomial in the Cartesian coordinates (x, y, z) followed by an exponential in r^2 (Equation 2.1.15). $e^{-\alpha r^2}$ is an analytically integrable term and is computationally much more efficient.

$$\boldsymbol{\chi_{\alpha,l_x,l_y,l_z}(x,y,z) = Nx^{l_x}y^{l_y}z^{l_z}e^{-\alpha r^2}} \qquad \textbf{(2.1.15)}$$

The value of $l_x + l_y + l_z$ determines what type the orbitals are. For example, l=1 is p orbital. The exponent α is optimized to provide the desired shape and energy of the wavefunction. χ can be either a single Gaussian functions or linear combinations of Gaussian functions. The shape difference of Slater type orbital (STO) and the optimized single Gaussian type orbital (GTO) with respect to hydrogen *1s* atomic orbital can be seen

in the following figure.

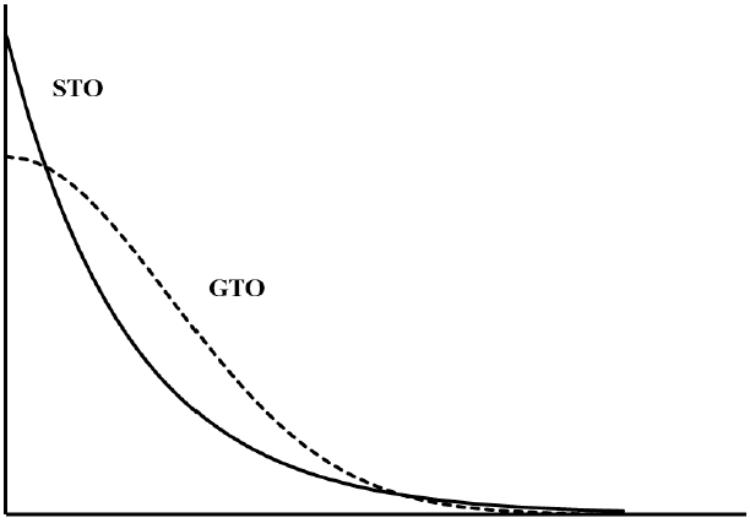

Figure 2.1 STO and GTO representation of hydrogen *1s* atomic orbital

Notice that in Figure 2.1, STO has an *s* cusp while GTO has zero slope at r=0. Therefore, single GTO does a bad job in terms of representing the gradient of electron density at or near the nucleus. Fortunately, a linear combination of Gaussian functions could be used to better mimic a Slater function. This combination has the following form:

$$\boldsymbol{\phi_\mu = \sum_{i=1}^{L} d_{i\mu} \phi_i(\alpha_{i\mu})} \qquad \textbf{(2.1.16)}$$

$d_{i\mu}$ is the expansion coefficient of the primitive Gaussian function ϕ_i. It has an exponent $\alpha_{i\mu}$. L is the number of functions in the expansion. It would be the most flexible and accurate way to use Gaussians in *ab initio* calculations if we allow $\alpha_{i\mu}$ and $d_{i\mu}$ to vary during the calculation. This kind of Gaussians are called un-contracted or primitive Gaussians. Obviously, calculations using un-contracted Gaussians are rather

computationally demanding. So contracted Gaussians are most often used in *ab initio* calculation. In a contracted function $\alpha_{i\mu}$ and $d_{i\mu}$ remain constant during the calculation.

Linear combinations of Gaussian functions used to create molecular orbitals represent a basis set. A minimal basis set is a representation that only comprises those functions required to accommodate all of the electrons in each atom. Quantum chemists found that at least three Gaussians are required to properly represent one STO. So the minimum that should be used in *ab initio* calculations are STO-3G basis set.

The STO-3G basis sets are well known to have several shortcomings. It cannot describe non-spherical molecular environments. All basis functions are defined to be spherical or the effect of their combination define a sphere. The second drawback is that basis functions are atom-centered and the two parameters $\alpha_{i\mu}$ and $d_{i\mu}$ are not allowed to vary during calculation. This really restricts their flexibility to contract in size to accommodate to the molecular environment, such as to describe electron distributions when forming and breaking bonds.

These shortcomings with STO-3G can be addressed by split-valence basis sets and polarization basis sets. Split-valence basis sets will use more than one contracted Gaussians to represent valence atomic orbitals. Take 6-31G for instance, six Gaussian functions are used to describe the core orbitals and the valence orbitals are split into two parts: three Gaussians for contracted part and one Gaussian for diffusion part.

The most common solution to the second drawback of minimal basis set is to introduce polarization effects into the basis set by providing p orbitals on hydrogen and d orbitals on main-group atoms where the valence electrons are of s and p type. For 6-31G, incorporation of polarization functions on heavy atoms can be represented by 6-31G(d)

and the use of polarization functions also on hydrogen and helium can be referred to 6-31G(d,p). This shape distortion can be seen in Figure 2.2 (Figure adapted from page 71, ref 63). 6-31+G(d,p) adds an additional single set of diffuse s and p Gaussian functions on heavy atoms to

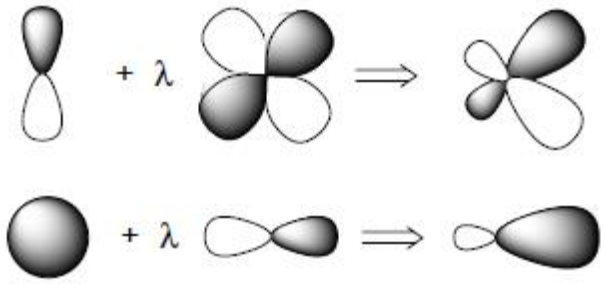

Figure 2.2 The addition of a $2p_x$ orbital to *1s* and $3d_{xy}$ orbital to $2p_z$ leads to orbital distortion

6-31G(d,p). That highly diffuse functions overcome the deficiency of so far described basis sets that are unable to deal with anions and molecules containing lone pairs in which electron density is relatively large for places that are far away from nuclear centers.

2.1.5 Hartree-Fock approximation

The calculations of molecular orbital and atomic orbitals are needed in the hydrogen molecule calculation. The Hartree–Fock method defines a term which is spin-orbital to approximate the one-electron wave function. For atomic orbital calculation, it is just an orbital for a hydrogenic atom. For molecular orbital calculation, it is typically a linear combination of atomic orbitals. We already know that for many-electron system, it is impossible to get the exact solution. How do we decide if one wavefunction is better than another? The variational theory states that the energy calculated from an approximation to the exact wavefunction will always be greater than the exact energy. Therefore, we can

determine one wavefunction is better than another if it gives a lower energy. Obviously, the best wavefunction will give a minimum energy. At a minimum, the derivative of the energy in terms of the nuclear coordinates, ∂E, will be zero.

The assumption that electrons move independently of each other was made when solving the electronic Schrödinger equation. But the problem is we want to find a solution that takes all electronic motions into account. So in practice, we assume individual electron in a spin orbital χ_i is in the average field of nuclei and the other electrons in their spin orbitals χ_j. The Hamiltonian operator for the electron in spin orbital χ_i contains core, Coulomb and exchange contribution to the energy. The result can be written in an equation that has the following form (Equation 2.1.17):

$$\left[-\frac{\mathbf{1}}{\mathbf{2}}\boldsymbol{\nabla}_{\boldsymbol{i}}^{\mathbf{2}}-\sum_{\boldsymbol{A}=\mathbf{1}}^{\boldsymbol{M}}\frac{\boldsymbol{Z_A}}{\boldsymbol{r_{iA}}}\right]\boldsymbol{\chi_i}(\mathbf{1})+\sum_{\boldsymbol{j}\neq\boldsymbol{i}}\left[\int \boldsymbol{d\tau_2}\boldsymbol{\chi_j}(\mathbf{2})\,\boldsymbol{\chi_j}(\mathbf{2})\frac{\mathbf{1}}{\boldsymbol{r_{12}}}\right]\boldsymbol{\chi_i}(\mathbf{1})$$

$$-\sum_{\boldsymbol{j}\neq\boldsymbol{i}}\left[\int \boldsymbol{d\tau_2}\boldsymbol{\chi_j}(\mathbf{2})\,\boldsymbol{\chi_i}(\mathbf{2})\frac{\mathbf{1}}{\boldsymbol{r_{12}}}\right]\boldsymbol{\chi_j}(\mathbf{1})=\sum_{\boldsymbol{j}}\boldsymbol{\varepsilon_{ij}}\,\boldsymbol{\chi_j}(\mathbf{1}) \qquad \textbf{(2.1.17)}$$

This integro-differential equation becomes more easier to illustrate with the introduction of core Hamiltonian operator $\mathcal{H}^{\text{core}}(1)$, Coulomb operator $\mathcal{J}_j(1)$ and exchange operator $\mathcal{K}_j(1)$:

$$\boldsymbol{\mathcal{H}^{\text{core}}}(\mathbf{1})=-\frac{\mathbf{1}}{\mathbf{2}}\boldsymbol{\nabla}_{\boldsymbol{i}}^{\mathbf{2}}-\sum_{\boldsymbol{A}=\mathbf{1}}^{\boldsymbol{M}}\frac{\boldsymbol{Z_A}}{\boldsymbol{r_{iA}}} \qquad \textbf{(2.1.18)}$$

$$\boldsymbol{\mathcal{J}_j}(\mathbf{1})\boldsymbol{\chi_i}(\mathbf{1})=\left[\int \boldsymbol{d\tau_2}\boldsymbol{\chi_j}(\mathbf{2})\frac{\mathbf{1}}{\boldsymbol{r_{12}}}\boldsymbol{\chi_j}(\mathbf{2})\right]\boldsymbol{\chi_i}(\mathbf{1}) \qquad \textbf{(2.1.19)}$$

$$\mathcal{K}_{\boldsymbol{j}}(\mathbf{1})\boldsymbol{\chi_i}(\mathbf{1})=\left[\int \boldsymbol{d\tau_2}\boldsymbol{\chi_j}(\mathbf{2})\frac{\mathbf{1}}{\boldsymbol{r_{12}}}\boldsymbol{\chi_i}(\mathbf{2})\right]\boldsymbol{\chi_j}(\mathbf{1}) \qquad \textbf{(2.1.20)}$$

The exchange operator $\mathcal{K}_j$ must be acted upon on χ_i because it exchanges the positon of electrons 1 and 2.

The Hartree-Fock equation then leads to the following form:

$$\left[\boldsymbol{\mathcal{H}}^{\mathbf{core}}(\mathbf{1}) + \sum_{\mathbf{j=1}}^{\mathbf{N}}\{\boldsymbol{\mathcal{J}}_{\boldsymbol{j}}(\mathbf{1}) - \mathcal{K}_{\boldsymbol{j}}(\mathbf{1})\}\right]\boldsymbol{\chi}_{\boldsymbol{i}}(\mathbf{1}) = \sum_{\boldsymbol{j}} \boldsymbol{\varepsilon}_{\boldsymbol{ij}}\, \boldsymbol{\chi}_{\boldsymbol{j}}(\mathbf{1}) \qquad \textbf{(2.1.21)}$$

It can be written in a more simple form[64]:

$$\mathfrak{f}_{\mathbf{i}}\boldsymbol{\chi}_{\boldsymbol{i}} = \sum_{\boldsymbol{j}} \boldsymbol{\varepsilon}_{\boldsymbol{ij}}\, \boldsymbol{\chi}_{\boldsymbol{j}} \qquad \textbf{(2.1.22)}$$

f is called the Fock operator. However, this equation don't seem to be practically useful. It is not an eigenfunction! The Fock operator acting upon orbital χ_i does not yield a constant multiplied by the orbital, but rather a series of orbital χ_j multiplied by some unknown parameter ε_{ij}. This reflects that the solutions to the Hartree-Fock equations are not unique. Fortunately, we could manipulate this equation mathematically so that the Lagrangian multipliers are zero unless *i*, *j* are the same. Thus, we could write up the Hartree-Fock equation in the form:

$$\mathfrak{f}_{\boldsymbol{i}}\boldsymbol{\chi}_{\boldsymbol{i}} = \boldsymbol{\varepsilon}_{\boldsymbol{i}}\boldsymbol{\chi}_{\boldsymbol{i}} \qquad \textbf{(2.1.23)}$$

Remember that when introducing these functions, each electron is assumed to move in the average field of nuclei and the other electrons. Any solution that is found by solving the equation for one electron will influence the solutions for the other electrons. The solution to treat this kind of situation is called the self-consistent field (SCF) approach. Initially, a set of trial solutions χ_i are given to the Hartree-Fork equation to calculate the Coulomb and exchange operators. Then the Hartree-Fock function is solved and output another set of solutions which are then used for the next function to be solved. By gradually

refining and adjusting the solutions to lower orbital energies, the SCF approach will get to the point that the energy is minimum. This is so called "self-consistent".[63]

The energy obtained by solving the Hartree-Fock equation is an upper bound to the true ground state energy of a molecule. In terms of the Hartree-Fock method, the lowest energy is at the Hartree-Fock limit and is obtained as the basis set approaches completeness. To get the energy lower than the Hartree-Fock limit, electron correlation must be incorporated into the calculation method.

So far there are four approximations discussed above. Born-Oppenheimer approximation, basis set approximation, LCAO approximation and the approximation that each electron moves independently from each other. The Hartree-Fock approximation is based on all these approximations.

The combination of Hartree-Fock and LCAO approximations leads to the following equation:

$$\mathrm{f_i}(\mathbf{1}) \sum_{v=1}^{K} \boldsymbol{c_{vi}} \emptyset_{v(1)} = \boldsymbol{\varepsilon_i} \sum_{v=1}^{K} \boldsymbol{c_{vi}} \emptyset_{v(1)} \qquad \textbf{(2.1.24)}$$

Multiplying each side by $\emptyset_{\mu(1)}$ and integrating yields to the matrix equation:

$$\sum_{v=1}^{K} \boldsymbol{c_{vi}} \int \boldsymbol{dv_1} \emptyset_{\mu(1)}\, \mathrm{f_i}(\mathbf{1}) \emptyset_{v(1)} = \boldsymbol{\varepsilon_i} \sum_{v=1}^{K} \boldsymbol{c_{vi}} \int \boldsymbol{dv_1}\, \emptyset_{\mu(1)} \emptyset_{v(1)} \qquad \textbf{(2.1.25)}$$

$\int dv_1 \emptyset_{\mu(1)}\, \emptyset_{v(1)}$ is the overlap integral between the two basis functions μ and v. Unlike molecular orbitals that are constrained to be orthonormal in the Hartree-Fock method, this integral does not have to be zero. Through a series of expansion and mathematical manipulations, each element $F_{\mu v}$ of the Fock matrix elements for a closed-shell system has the form

$$\boldsymbol{F_{\mu v} = H_{\mu v}^{core} + \sum_{\lambda=1}^{K} \sum_{\sigma=1}^{K} P_{\lambda\sigma} \left[(\mu v|\lambda\sigma) - \frac{1}{2} (\mu\lambda|v\sigma) \right]} \quad \textbf{(2.1.26)}$$

This is the Fock matrix expression in the Roothaan-Hall equations.[63] $(\mu v|\lambda\sigma)$ are two-electron integrals. *P* is the charge density matrix. Its element contains the product of two molecular orbital coefficients summed over all occupied molecular orbitals. This leads to the electron density which will be discussed later on.

$$\boldsymbol{P_{\lambda\sigma} = 2 \sum_{i=1}^{N/2} c_{\lambda i} \, c_{\sigma i}} \quad \textbf{(2.1.27)}$$

The Roothaan-Hall equations can be simply written up as matrix equations:

$$\textbf{FC = SCE} \quad \textbf{(2.1.28)}$$

F is the Fock matrix, which is the same as the Hamiltonian in the Schrödinger equation, **E** are diagonal matrix of orbital energies, S is the overlap matrix.[64]

Methods involving solving Roothaan-Hall equations are termed as Hartree-Fock models. They are both size consistent and variational. Hartree-Fock calculations usually yield at least qualitative accuracy in energy difference calculations. Hartree-Fock models interpret energies from purely analytical methods, so do the first and second energy derivatives. This is very good for geometry optimization and determination of vibrational frequencies. Geometry optimization and vibrational frequencies use first derivative and second derivatives respectively.

2.1.6 Electron Correlation

The Hartree-Fock method treats electrons independent of each other. They replace "instantaneous interactions" between electrons by interactions between a particular electron and the mean field created by all the other electrons. This results in overestimation

of electron-electron repulsion energy and overall too high for total energy. Electron correlation accounts for the neglect of instantaneous electron-electron correlation interactions of the Hartree-Fock method. The correlation energy is defined as the difference between energy calculated with exact wave-function and energy from using Hartree-Fock function.

$$\boldsymbol{E_{corr} = E_{exact} - E_{HF}} \qquad \textbf{(2.1.29)}$$

In general, correlation energy is obtained by adding additional Slater determinants to our expansion of ψ.

$$\boldsymbol{\psi_{el} = d_0 \emptyset_{HF} + \sum_{I=1} d_i \emptyset_i} \qquad \textbf{(2.1.30)}$$

Different correlation models such as configuration interaction models and Møller-Plesset models differ in how they choose which $\emptyset_i$ to include in the model and in how they calculate the coefficients d_i. As correlation models mix ground-state and excited-state wavefunctions, they are much more costly than Hartree-Fock models. Density functional theory uses an approximate correlation term in an explicit manner. They are not significantly more costly than Hartree-Fock models. Obviously, the accuracy of density functional models relies on the term used.

It will be much clearer when we look at the following two-dimensional diagram on which we can find all possible calculation models (Figure 2.3). The top right corner indicates the exact solution to the Schrödinger equation, which cannot be achieved in practice.

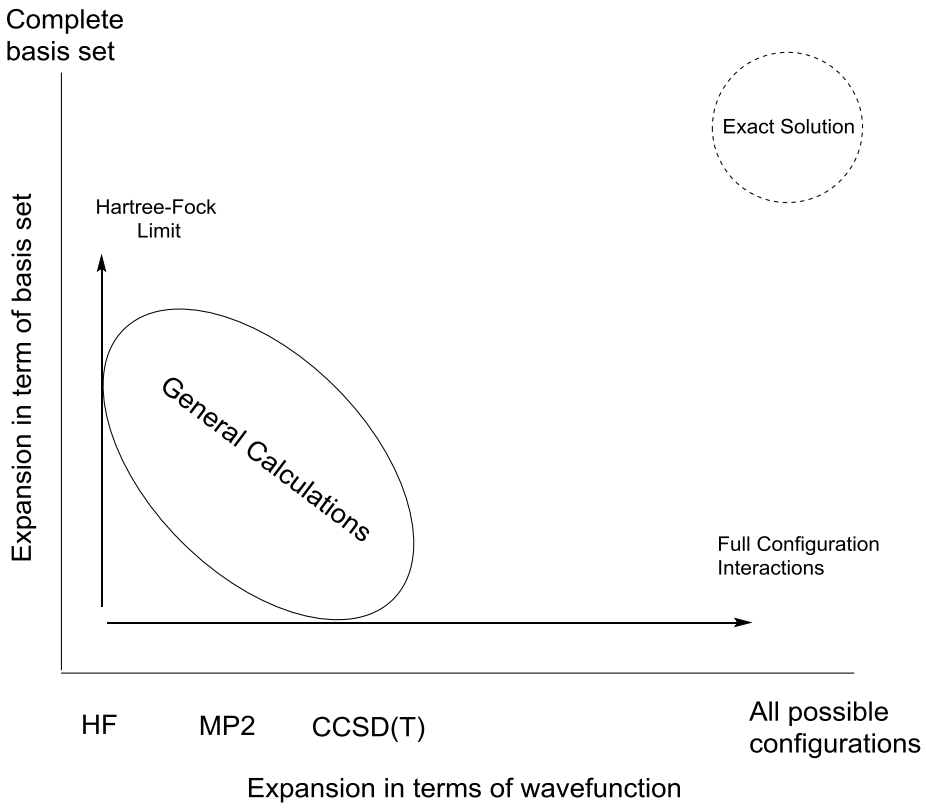

Figure 2.3 Two dimensional graph where all possible calculation methods can be located.

2.1.7 Density Functional Theory

So far, the methods we have been discussing can be categorized as "Wavefunction methods". The energies and properties obtained are based on solving for the electron wavefunction. Another strategy dealing with electron correlation is the density functional theory, which instead solves for the electron density $\rho(r)$,[30] as opposed to the many-electron wavefunctions $\psi(r_1,r_2,r_3\ldots)$. Many-electron wavefunction methods and DFT methods do have some similarities. They are both based on single-electron orbitals and are done in an SCF way. In 1964, Hohenberg and Kohn stated that energy is a functional of electron density, $E[\rho]$.[30] The exchange and correlation energies of a uniform electron gas can be obtained by calculating its density. This is for ground-state energy only, but exact $\rho(r)$ can

minimize E[ρ]. Later in 1965, Kohn and Sham further elaborated this theory by giving the form,[66]

$$\boldsymbol{E = E_T + E_V + E_J + E_{XC}} \qquad \textbf{(2.1.31)}$$

Where E is the ground-state energy, E_T is a sum of kinetic energy, E_V is the electron-nuclear interaction energy, E_J is the Coulomb energy and E_{XC} is the exchange and correlation energy.[66]

Other than E_T, all the other terms are based on the total electron density ρ(r).

$$\boldsymbol{\rho(r) = 2\sum_i^{orbitals}|\psi_i(r)|^2} \qquad \textbf{(2.1.32)}$$

$\psi_i(r)$ are the Kohn-Sham orbitals. Those energy components can be written as follows.

$$\boldsymbol{E_T = \sum_\mu^{basis}\sum_v^{functions}\int \emptyset_\mu(r)\left[-\frac{1}{2}\nabla^2\right]\emptyset_v(r)dr} \qquad \textbf{(2.1.33)}$$

$$\boldsymbol{E_V = \sum_\mu^{basis}\sum_v^{functions} P_{\mu v}\sum_A^{nuclei}\int \emptyset_\mu(r)\left|\frac{Z_A}{|r-R_A|}\right|\emptyset_v(r)dr} \qquad \textbf{(2.1.34)}$$

$$\boldsymbol{E_J = \frac{1}{2}\sum_\mu^{basis}\sum_v\sum_\lambda^{functions}\sum_\sigma P_{\mu v}P_{\lambda\sigma}(\mu v|\lambda\sigma)} \qquad \textbf{(2.1.35)}$$

$$\boldsymbol{E_{XC} = \int f(\rho(r), \nabla\rho(r), \dots)dr} \qquad \textbf{(2.1.36)}$$

P is the density matrix in equation 2.1.26 and $(\mu v|\lambda\sigma)$ are the two-electron integrals. f in E_{XC} is the exchange and correlation functional, which is a function of electron density and maybe the gradient of density as well.

E_V and E_J are solved with Kohn-Sham orbitals which are analogous to the LCAO approximation using a set of single-electron spin orbitals solved by SCF approach. The

exchange/correlation component has an advantage over Hartree-Fock as dynamic correlation energy is included in the functional. However, the exact form of this functional is so far unknown.[67] While many approximations such as local density approximation (LDA) and generalized gradient approximation (GGA) has been used, there is still no systematical way to improve it.[68] So it lacks the systematics that characterize wavefunction methods.

In practice, most implementations of density functional theory solve equation 2.1.30 by dividing the problem into two parts. The first part is to use the same analytical procedures applied to Hartree-Fock except the exchange/correlation functional. The local density model and non-local density models such as BLYP and BP just use the Hartree-Fock Coulomb term $\mathcal{J}_j$ and exchange term $\mathcal{K}_j$. Hybrid density functional models, such as B3LYP use Hartree-Fock exchange term. The second part is to tackle the exchange/correlation functional. So far there are no analytical procedures that have been developed to compute the integrals. In the practical DFT implementations, numerical integration using grid specification is an important and active area. To make DFT work more applicable, "pseudoanalytical" procedures have been developed to calculate the first and second energy derivatives which are fundamental to the determination of transition-state geometries and vibrational frequencies.

In terms of the computation speed, DFT methods are similar to Hartree-Fock methods. Most DFT methods involve some empirical parameterization which make them more practical from small to large molecules. Both lead to its popularity across the whole chemistry world.

2.1.8 Semi-empirical models

Semi-empirical models directly inherit from Hartree-Fock methods. They treat valence electrons only which can reduce the size problem. The basis set is also set to a minimal representation for valence. To further reduce the overall computational cost, empirical parameters are introduced to reproduce a wide range of experimental data such as heats of formation, dipole moments and equilibrium geometries. Popular semi-empirical methods such as AM1 and PM3 models use fundamentally the same approximations but just different parameterizations.

2.2 Molecular Mechanics

Quantum Mechanics deals with electrons in a system. Molecular mechanics (also known as force field methods) describes molecules as a collection of spatial parameters of atoms, including bonds, angles, dihedral angles and non-bonded interactions such as van der Waals and Coulombic interactions. They are fundamentally different from each other. There is no way that molecular mechanics could predict properties that are based on electron distribution. Transferability is a core attribute of a force field. A high degree of transferability enables a force field that is developed over a relatively small amount of cases to be applied to a broad range of cases, including from small molecules to large molecules such as proteins.

A simple force field (Equation 2.2.1) can be expressed as an equation that has four components including both intra and inter-molecular forces (Equation 2.2.2-2.2.5)[63]

$$\boldsymbol{E_{total} = E_{bonds} + E_{angles} + E_{torsions} + E_{non-bonded}} \qquad \textbf{(2.2.1)}$$

$$\boldsymbol{E_{bonds} = \sum_{bonds} \frac{k_i}{2} (r - r_0)^2} \qquad \textbf{(2.2.2)}$$

$$\boldsymbol{E_{angles} = \sum_{angles} \frac{k_j}{2}(\theta - \theta_0)^2} \quad \textbf{(2.2.3)}$$

$$\boldsymbol{E_{torsions} = \sum_{torsions} \frac{V_n}{2}\left(1 + cos(n\omega - \gamma)\right)} \quad \textbf{(2.2.4)}$$

$$\boldsymbol{E_{non-bonded} = \sum_{i=1}^{N} \sum_{j=i+1}^{N} \left(4\varepsilon_{ij}\left[\left(\frac{\sigma_{ij}}{r_{ij}}\right)^{12} - \left(\frac{\sigma_{ij}}{r_{ij}}\right)^{6}\right] + \frac{q_i q_j}{4\pi\varepsilon_0 r_{ij}}\right)} \quad \textbf{(2.2.5)}$$

k_i is the force constant and V is the torsional barrier height.

The first three components are all summations over bond parameters, including bond stretching, bond angles and torsion angles. The fourth component is the non-bonded term which uses a sum of van der Waals interactions and electrostatic interactions that are modelled by Lennard-Jones potential and Coulomb potential. When dealing with the hydrogen-bonding effect, some force fields replace the Lennard-Jones terms with an explicit hydrogen-bond term.

Different force fields differ mainly on the non-bonded term. The Lennard-Jones potential (12-6-term) models the repulsive potentials (r^{-12} term) and attractive van der Waals potentials (r^{-6}) which can be represented as a potential energy curve with a well depth of $-\varepsilon$ and an equilibrium radius of σ.

The all-atom optimized potentials for liquid simulations, denoted as OPLS-AA, is one of the most popular force fields. It has been demonstrated to reproduce a wide range of experimental properties of solvents, organic and biomolecular systems.[69] It is developed and then implemented in BOSS and MCPRO programs by Prof. William L. Jorgensen at Yale University. It is very similar to the general force fields form in Equation 2.2.1. The non-bonded term can be expressed as Equation 2.2.6:

$$E_{non-bonded} = \sum_{i<j} f_{ij} \left(4\varepsilon_{ij} \left[\left(\frac{\sigma_{ij}}{r_{ij}} \right)^{12} - \left(\frac{\sigma_{ij}}{r_{ij}} \right)^{6} \right] + \frac{q_i q_j}{4\pi\varepsilon_0 r_{ij}} \right) \quad \textbf{(2.2.6)}$$

f_{ij} = 0.5 for 1, 4-interactions and 1.0 for the other cases.[70]

The OPLS-AA force field[71,72] is parameterized to reproduce experimental properties including density and heat of vaporization. These properties represent the molecular sizes and intermolecular interactions. Therefore, being able to reproduce those properties could determine whether a force field is applicable or not.

2.3 Mixed Quantum and Molecular Mechanics Methods (QM/MM)

Nowadays, chemists are getting interested in larger and larger systems which involve hundreds and even thousands of atoms. It is not realistic to model chemical reactions in such systems using purely quantum mechanics or molecular mechanics methods. While great accuracy may be achieved, treating the systems using only QM will be very time consuming. The algorithms complexity of the simplest *ab-initio* calculations is $O(N^3)$. N is actually the number of basis functions which are no less than the number of atoms. As chemical reactions usually involve bond breakage and formation, we cannot treat the whole system using only molecular mechanics as it is not based on electron distribution.

However, this problem can be solved by dividing the system into three parts. A small part of the system that we are mainly interested in is treated with quantum mechanics. The non-reactive region, usually the solvent phase or non-active region of protein, is treated with molecular mechanics. The interface can be treated with QM/MM. Thus, the total energy can be expressed by three parts.

$$E_{total} = E_{QM} + E_{MM} + E_{QM/MM} \quad \textbf{(2.3.1)}$$

In the present study, QM part is treated with PDDG/PM3 semi-empirical method and MM is OPLS-AA force field. The QM/MM energy can be calculated using the similar way as non-bonded term in OPLS-AA force field.

$$\mathbf{E_{QM/MM}} = \sum_{\mathbf{I}}^{\mathbf{solute}} \sum_{\mathbf{J}}^{\mathbf{solvent}} \left[\frac{\alpha q_i^{CMX} q_j e^2}{r_{ij}} + 4\varepsilon_{ij} \left[\left(\frac{\sigma_{ij}}{r_{ij}} \right)^{12} - \left(\frac{\sigma_{ij}}{r_{ij}} \right)^{6} \right] \right] \qquad \textbf{(2.3.2)}$$

α is the scaling factor of charge model. When used in solution it is 1.14 for charge model 1 (CM1) and is 1.15 for charge model 3 (CM3).[73] These scaling factors have great accuracy and result in errors about 1 kcal·mol^{-1}.

2.4 Statistical Mechanics

The connection between microscopic and macroscopic system is provided by statistical mechanics.

At any specific temperature there is a distribution of molecules in all quantum energy states. The probability P of a molecule found in a state with energy Ɛ at temperature T can be expressed as a function of a Boltzmann factor.

$$P \propto e^{-\varepsilon/kT} \qquad \textbf{(2.4.1)}$$

According to this formula, the most possible energy of a molecule is not necessarily the one with the lowest energy.

The most important feature in statistical mechanics is the partition function. This is just like wavefunction in quantum mechanics. The partition function enables the calculation of all macroscopic functions in statistical mechanics.

The partition function can be written as a summation over all energy levels,

$$q = \sum_{i=levels}^{\infty} g_i \, e^{-\varepsilon_i/kT} \qquad (2.4.2)$$

Where g_i is the degeneracy factor which indicates how many states there are with the same energy level ε_i.

The partition function q is the function for a single molecule. Because thermodynamic values are obtained as molar quantities, the corresponding quantity Q is q^N for a collection of N non-interacting, different particles (ideal gas). If the particles are interacting (condensed phase), the corresponding partition function Q must be obtained by a summation over all energy states E_i.

$$Q = \sum_{i=levels}^{\infty} e^{-E_i/kT} \tag{2.4.3}$$

The partition function Q can be then applied to thermodynamic functions, such as the internal energy U, Helmholtz free energy A, enthalpy H, entropy S and Gibbs free energy G.

$$U = kT^2 \left(\frac{\partial lnQ}{\partial T}\right)_V \tag{2.4.4}$$

$$A = -kTlnQ \tag{2.4.5}$$

$$H = U + PV = kT^2 \left(\frac{\partial lnQ}{\partial T}\right)_V + kTV \left(\frac{\partial lnQ}{\partial V}\right)_T \tag{2.4.6}$$

$$S = \frac{U-A}{T} = kT \left(\frac{\partial lnQ}{\partial T}\right)_V + KlnQ \tag{2.4.7}$$

$$G = H - TS = kTV \left(\frac{\partial lnQ}{\partial V}\right)_T - kTlnQ \tag{2.4.8}$$

In order to calculate the partition function q or Q, we need to know all possible quantum states of the system. These can be calculated by solving the Schrödinger function. However, this approach is only feasible for di- and triatomic systems. For a polyatomic molecule, the rigid-rotor harmonic-oscillator approximation has to be made in order to calculate the energy levels for a single conformation. In this approximation, the electronic, vibrational and rotational degrees of freedom are assumed to be separable. Thus, the

partition function q is then a product of electronic, rotational, vibrational and translational partition functions (equation 2.4.9). The total energy of the system is then the sum of electronic, rotational, vibrational and translational energies (equation 2.4.10).

$$q_{tot} = q_{elec} q_{vib} q_{rot} q_{trans} \tag{2.4.9}$$

$$\varepsilon_{tot} = \varepsilon_{elec} + \varepsilon_{vib} + \varepsilon_{rot} + \varepsilon_{trans} \tag{2.4.10}$$

2.5 Many body thermodynamics

For a system having only non-interacting molecules (ideal gas), the partition function can be obtained accurately by the rigid-rotor harmonic-oscillator approximation from geometry and vibrational frequencies. For liquid and solutions, the thermodynamic quantities derived from the partition function must be obtained by a sampling of the phase space. Simulation is such sampling of a system at a finite temperature.

Monte Carlo is one of the major methods to generate an ensemble. A Monte Carlo simulation integrates over completely random configurations. If the energy of the new configuration is higher, the Boltzmann factor $e^{-\Delta E/kT}$ is calculated and then compared to a random number between 0 and 1. If the Boltzmann factor is larger than this random number, the new configuration is confirmed. Otherwise, the old geometry is retained for the next sampling. The Metropolis procedure[65] chooses only those configurations that obey Boltzmann distribution. When the system attempts to move from configuration *i* to configuration *j*, it is either accepted or rejected. In order to have a higher acceptance ratio, the step size has to be small. The Metropolis selection algorithms ensures that a proper ensemble can be generated. The geometry perturbations may be carried out in both internal and Cartesian coordinates. It is quite convenient to fix one degree of freedom such as torsional angle.

Chapter 3 Solvent Effects for Regioselective Aza-Michael Addition to Enone Acceptors: An Experimental and Theoretical Study

3.1 Abstract

Aza-Michael additions of amine to 5-nitronaphthalene-1, 4-dione acceptor (Scheme 3.1) take place in a highly regioselective manner, which is determined by which solvent is employed. High yield of 2-amino-1, 4-dione was obtained when using polar solvents such as water and ionic liquids. A reaction in dichloromethane, on the other hand, finishes up with 3-amino-1, 4-dione as the major product. In order to understand the solvent effects and the reaction mechanism, both *ab initio* and QM/MM calculations were performed in this case. The reaction is a two-step process, involving a tandem aza-Michael addition followed by an intramolecular hydrogen transfer. The second step was found to be the rate-determining-step. Moreover, water plays an essential role in the hydrogen transfer step by lowering the activation energy through hydrogen bonding.

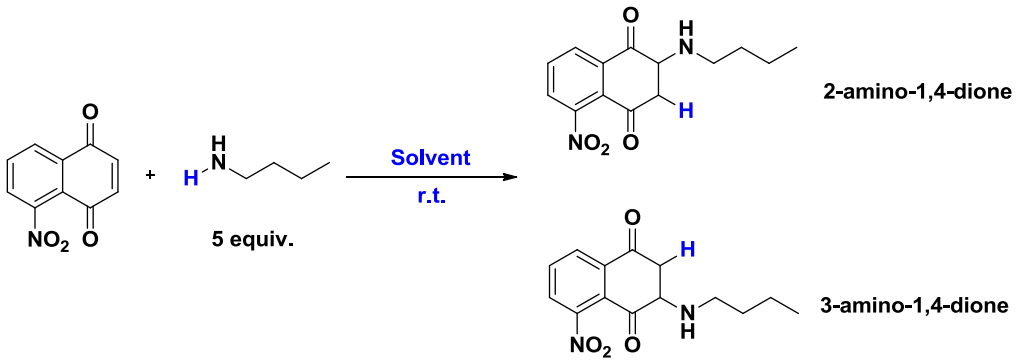

Scheme 3.1 Aza-Michael addition of n-butylamine to 5-nitronaphthalene-1,4-dione acceptor

3.2 Computational Methods

Reactants and transition states were located in 725 explicit solvent molecules represented using the TIP4P water model[74] and the OPLS-AA force field for non-aqueous

solutions.[75,76] The solutes were treated using the PDDG/PM3 semi-empirical QM method, [77]which has been reported to give excellent results for a wide variety of organic and enzymatic reactions in the solution phase.[78] Calculations of atomic charges and QM energy are performed for each attempted move of the solute, which happens every 100 configurations. CM3 charges[79] were obtained for the solute with a scaling factor of 1.14 for electrostatic contributions to the solute-solvent energy. Lennard-Jones interactions between solvent and solutes atoms were taken into account using OPLS parameters. This combination minimizes errors in the computed free energies of hydration for a PM3-based method.[80] Free energy changes were calculated using free energy perturbation (FEP) theory in conjunction with isothermal-isobaric (NPT) ensemble Metropolis Monte Carlo simulations at 25 °C and 1 atm. The starting geometry for solute of the nucleophilic addition step was determined by using PDDG/PM3 method. The hydrogen transfer step was originally determined by M06-2X/6-31+G(d,p) geometry optimization. Each FEP calculation entailed ca. 10 million configurations of equilibration and 20 million configurations of averaging at the increments of 0.01Å for the making/breaking bond distances. Double wide sampling was used to increase computing efficiency.

The BOSS program was used to carry out all QM/MM reactions from the stored and custom-made solvent boxes.[81] All solvents were fully flexible, i.e., all bond stretching, angle bending, and torsional motions were sampled, with the exception of water, acetonitrile, and methanol,[82] which already exist in the BOSS as fixed united-atom solvents. Periodic boundary conditions have been applied to tetragonal boxes containing 725 solvent molecules. Solute-solvent and solvent-solvent cutoffs of 12 Å were used with quadratic feathering of the intermolecular interactions with 0.5 Å of the cutoff. The BOSS program

sets the ranges for bond stretching and angle bending automatically on the basis of force constants and temperature. All QM/MM/MC calculations were run on computers located at the Alabama Supercomputer Center.

For comparison, AM1 and PDDG semi-empirical methods and B3LYP, M06-2X density functional methods in the 6-31+G(d,p) basis set were also used to optimize geometries in vacuum, acetonitrile, ethanol, dichloromethane, 2-propanol and water using Gaussian 09.[83] The effect of solvent was explored by full DFT geometry optimizations using the conductor-like polarizable continuum model (CPCM).[84] Frequency calculations were performed in order to verify all stationary points as minima for ground states or as saddle points for transition structures. All calculations were run on computers located at the Alabama Supercomputer Center.

3.3 Results and Discussion

The aza-Michael additions of n-butylamine to 5-nitronaphthalene-1,4-dione have two observed products (Scheme 3.1). Both conventional solvents and greener solvents including water and various ionic liquids were used to explore the solvent effects. Aza-Michael addition reactions usually go through two steps: nucleophilic addition of amine onto double bond and then intramolecular hydrogen transfer. The proposed reaction mechanism in the present work fits to the classical Michael addition mechanism (Scheme 3.2). The reaction was calculated in water initially. To get a starting geometry of TS1 for the QM/MM calculations, the PDDG/PM3 method was employed in Gaussian 09,[83] coupled with conductor-like polarizable continuum model for water. TS1 was confirmed by single imaginary frequency with a large value using both methods (Figure 3.1). Then the two TS1 structure coordinates were transformed into BOSS z-matrix, followed by the

QM/MM calculations in the BOSS program. The free energy map for TS1 were computed by perturbing the reacting bond distance R_{CN} via potentials of mean force (PMF) calculations in increments of 0.01 Å. The results are summarized in Figure 3.1.

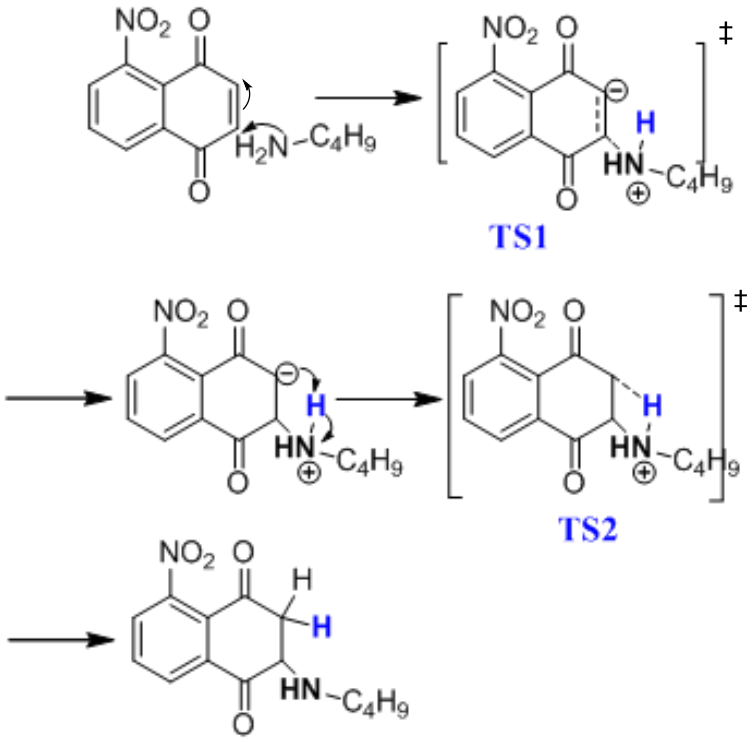

Scheme 3.2 Proposed aza-Michael addition mechanism

Clearly, attacking at 3-C should be favored from results predicted by QM/MM calculation, as the potential energy barrier for attacking at 2-C is larger than that for attacking 3-C by 17 kcal/mol. Both attacks resulted in a zwitterionic intermediate in which R(C-N) is

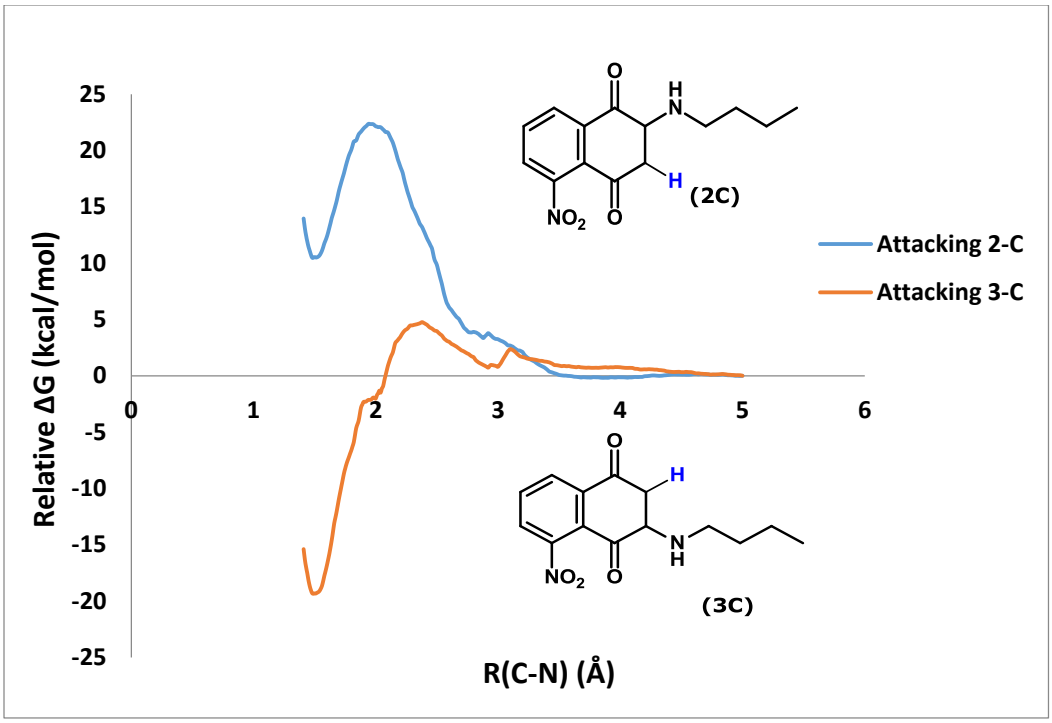

Figure 3.1 Free energy curve for TS1 from attacking 2-C and 3-C

about 1.5 Å. Surprisingly, the intermediate formed by attacking 3-C is 30 kcal/mol more stable than that attacking 2-C. After double checking to make sure no crash happened during QM/MM calculations, the results seem to be unreasonable. When carefully examining the two reactants when R(C-N) is 5 Å, we found that the structures of 5-nitronaphthalene-1,4-dione in two different attacks are different from each other. For 3-C attacking, the ring is twisted just like the structure shown in Figure 3.2 II. The ring structure should not be twisted as the optimized geometry has a boat-like flat ring. For 2-C attacking, on the other hand, the ring is as flat as that shown in Figure 3.2 I. Without having a nearly the same starting geometry for 5-nitronaphthalene-1,4-dione in both attacks, the results are not that trustable.

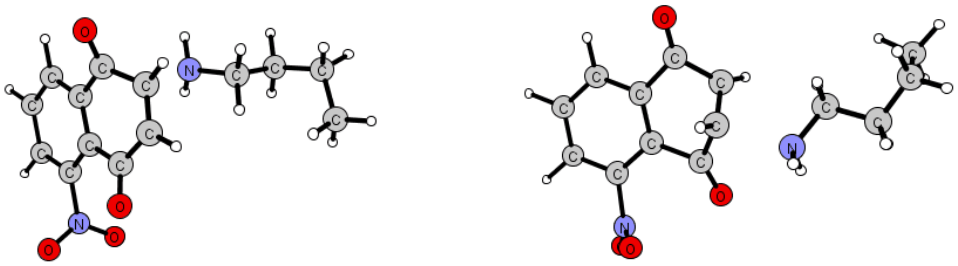

I **II**

Figure 3.2 TS1 for amine attacking 2-C of 5-nitronaphthalene-1,4-dione(I) and 3-C of 5-nitronaphthalene-1,4-dione (II)

As most semi-empirical methods including AM1 partly or completely omit electron correlation, these methods tend to overestimate the energy. Employing PDDG/PM3 generally improves the accuracy over the standard NDDO schemes, e.g. PM5, PM3, AM1 and MNDO.[85] These semi-empirical molecular orbital methods, while having different accuracy, seem to be practical for the calculation of large molecules. However, a key problem is the poor performance of current semi-empirical methods for non-covalent interactions, especially hydrogen-bonding.[86,87] This generally needs very high-level quantum chemical methods such as DFT. It has been reported that H-bonding can greatly influence the orientation of the transition structure.[88] In water, the ubiquitous H-bonding interactions may somehow play a role in the formation of the transition structure. Thus, H-bonding effect must be taken into account in the calculation.

DFT is generally accurate for the prediction of transition structures. It performs exceptionally well for molecular structure with much reduced computational effort than traditional *ab initio* methods. However, a recently published paper regarding the poor performance of B3LYP for the relative energy computations ended the happy days of its usage.[89] It shows its shortcomings in studies on, for example, the enthalpies of formation for chain hydrocarbons and the energy difference of propyne versus alkene (propyne is more stable by 1.4 kcal mol^{-1} under standard condition, whereas all established DFT methods give the opposite energy ordering with considerable error bars[90]). For B3LYP, it neglects long-range correlation (mostly van der Waals dispersion) and does not appropriately include medium-range correlation. A thorough computational study of the pair correlation energies (at the spin-component-scaled MP2 level of theory)[91] shows that it is non-local medium-range interactions (1.5-3.5 Å) that is responsible for rationalizing the energy differences. These findings explain why M05-2X could predict the energy difference very well, as it uses new functional forms for the dependence of the functional on the density gradient and kinetic energy density in both the exchange and correlation functionals.[92] M06-2X was then parameterized to be particularly suitable for main group thermochemistry, kinetics and no-covalent interactions. It includes van der Waals dispersion.[93] Our calculated results indicated that AM1, PDDG/PM3, B3LYP/6-31+G(d,p) overestimate energy (Table 3.2). PDDG/PM3 shows improvement over AM1. M06-2X gave lowest energy as it is implemented to incorporate van der Waals dispersion.

Table 3.1. Free energy of activation, $\Delta G^{\neq}$(kcal/mol) at 25 °C for the nucleophilic addition step of n-butylamine to 5-nitronaphthalene-1,4-dione from semi-empirical and DFT calculations in water, CPCM

	ΔG(kcal/mol) in water	
	TS1_2C	**TS1_3C**
AM1	32.1	32.5
PDDG/PM3	25.6	28.0
B3LYP/6-31+G(d,p)	26.0	26.1
M062X/6-31+G(d,p)	18.9	18.1

It has been demonstrated that the hydrogen transfer step in aza-Michael addition is usually the rate-determing-step.[88,94] Therefore, TS2 calculation became our first priority. As QM/MM/Monte Carlo simulation of transition structure is computationally demanding, a thorough QM calculation was undertaken prior to QM/MM. Semi-empirical calculations using AM1, PDDG/PM3 methods and DFT calculations using B3LYP/6-31+G(d,p) and M06-2X/6-31+G(d,p) were carried out in gas-phase and in water by using the CPCM continuum model (Table 3.2). In gas-phase, the activation barrier difference for TS2 formed by attacking 2-C and 3-C is within the calculation error range. In water, M06-2X gave almost identical ΔG values for the transition states, although TS2_2-C is slightly favored using other methods.

Notice that in Table 3.2, the calculated ΔG values are very high. It is about 40 kcal/mol as calculated by M06-2X/6-31+G(d,p), which indicates that hydrogen transfer in the second step of tandem aza-Michael addition requires a lot of energy. This is in agreement with literature results.[88,94] Fustero et al.[88] reported that trimethylamine can assist the hydrogen transfer for the tandem aza-Michael addition to acrylamide acceptors using B3LYP/6-31+G(d,p) method (Figure 3.1). Okumoto[94] performed a theoretical study of

curing reactions of maleimide resins through Michael additions of amines. Another amine eases the hydrogen transfer as it reduces the strain of TS (Figure 3.2). TS2 is less strained than TS1 as it has a nearly linear hydrogen bond. NHN angle α is 163.2^{o} in TS2 versus 110.4^{o} in TS1. Ea(TS2) = 11.6 kcal/mol is much smaller than Ea(TS1) = 30.1 kcal/mol owing to the stabilization of the linear hydrogen bonds.

Table 3.2. Free Energy of Activation, $\Delta G^{\neq}$(kcal/mol) at 25 $^{\circ}$C for the hydrogen transfer step of n-butylamine to 5-nitronaphthalene-1,4-dione from semi-empirical and DFT calculations in water (CPCM) and gas-phase

	ΔG‡(kcal/mol)			
	In water		**In gas-phase**	
	TS2_2-C	**TS2_3-C**	**TS2_2-C**	**TS2_3-C**
AM1	47.2	48.5	50.3	49.4
PDDG/PM3	33.4	37.0	40.4	40.3
B3LYP/6-31+G(d,p)	47.8	50.0	51.5	52.1
M062X/6-31+G(d,p)	39.0	39.4	42.0	41.0

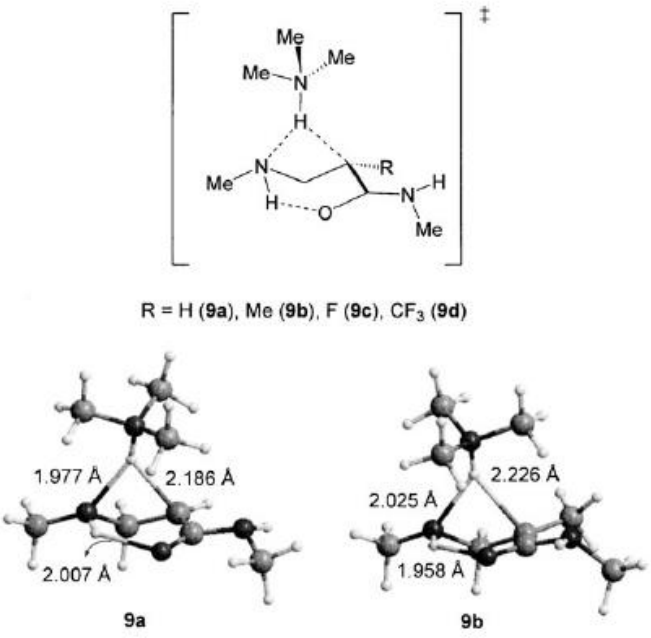

Figure 3.1 Trimethylamine assisting the hydrogen transfer for the tandem aza-Michael addition to acrylamide acceptors using B3LYP/6-31+G(d,p) method (Figure adapted from ref [88])

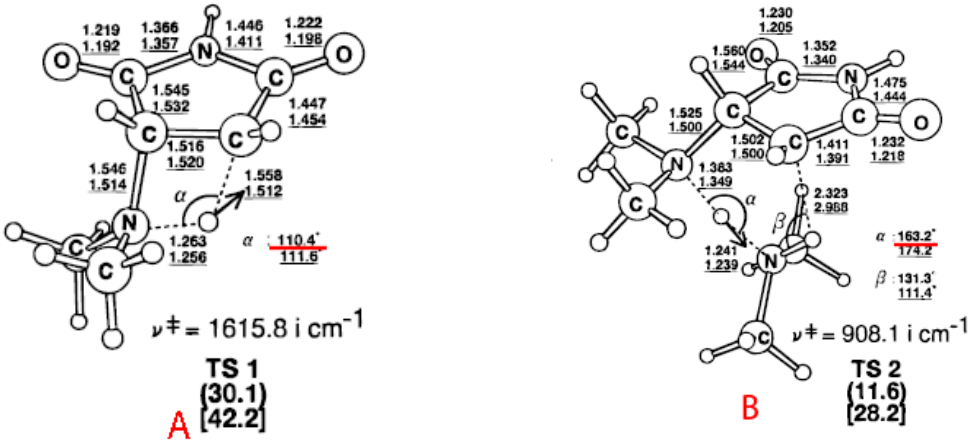

Figure 3.2 TS with (B) and without amine (A) assisting hydrogen transfer. (electronic energies), [Gibbs free energies](Figure adapted from ref [94])

It has been reported that water can help the 1,3-hydrogen transfer and lower the activation barrier.[95,96] Yu et al performed a joint computational and experimental study, showing that water could assist the intramolecular [1,2] proton shift in the Lu (3+2) cycloaddition. The generally accepted [1,2] proton shift is impossible due to the very high activation barrier of 39.6 kcal/mol required for this process. Experiments and calculations revealed that water assists this process with an activation free energy of 7.7 kcal/mol. Yu also performed a DFT study (B3LYP/6-31G*, SDD for Au) of the mechanisms of in water Au(I)-catalyzed tandem [3,3]-rearrangement/nazarov reaction/[1,2]-hydrogen shift of enynyl acetates. The water-catalyzed [1,2]-hydrogen shift is very efficient with activation free energies of 16.4 kcal/mol (using one water as the catalyst) and 13.0 kcal/mol (using a three-water cluster as the catalyst). Through all these two cases, water seems to act as a proton shuttle.

The following water assisted hydrogen transfer calculation was inspired by these two papers. Figure 3.3 shows TS2_2-C and TS2_3-C obtained with and without water assisted using M06-2X/6-31+G(d,p) method. There is less ring strain for the water assisting proton migration. Additionally, there is one extra NHO hydrogen bond for TS2_2-C, which could explain why TS2_2-C is favored over TS2_3-C in terms of activation energy.

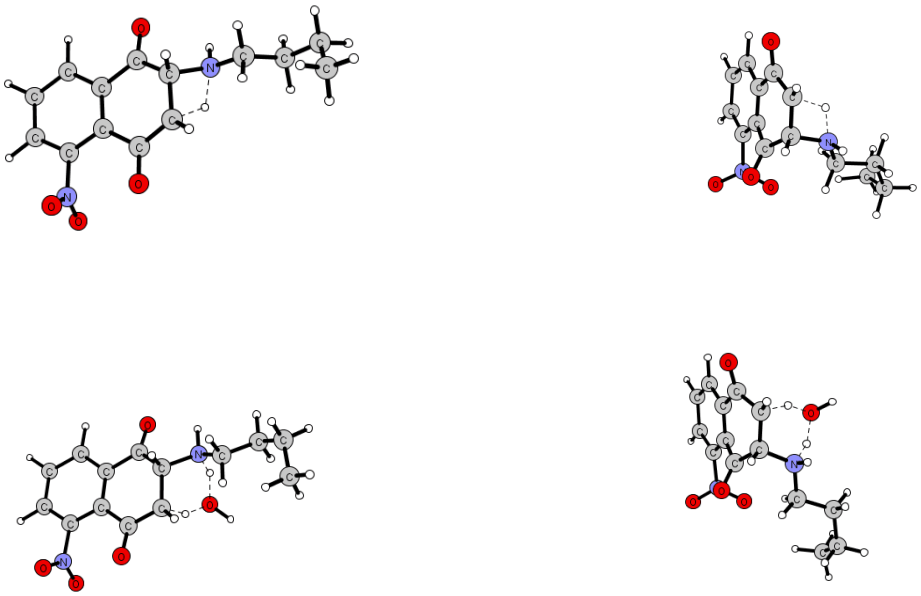

Figure 3.3 TS2_2-C and TS2_3-C obtained without and with water assisting using M06-2X/6-31+G(d,p) method

Table 3.3. Free energy of activation, ΔG≠(kcal/mol) at 25 ˚C for the water assisted hydrogen transfer of n-butylamine to 5-nitronaphthalene-1,4-dione from semi-empirical and DFT calculations in water and gas-phase

	ΔG≠(kcal/mol)			
	In water		**In gas-phase**	
	TS2_2-C	**TS2_3-C**	**TS2_2-C**	**TS2_3-C**
AM1	56.2	59.7	62.2	63.1
PDDG/PM3	44.8	50.7	48.0	49.2
B3LYP/6-31+G(d,p)	37.8	42.6	38.8	44.1
M06-2X/6-31+G(d,p)	26.4	32.4	27.4	30.3

Table 3.3 gave a summary of free energy of activation for water-assisted hydrogen transfer in vacuum and water. Semi-empirical methods overestimated the activation energy. DFT methods gave lower energies which implies a better performance in terms of H-bonding. In aqueous phase calculations using the M06-2X/6-31+G(d,p) method, calculated $\Delta G^{\neq}$ of TS2_2-C is 6 kcal/mol lower than that of TS2_3-C. The lower energy of TS2_2-C can be explained by an additional H-bond which is shown in Figure 3.3. The H-bond distance is 2.01 Å, whereas in TS2_3-C, there is no such hydrogen bonding interaction. Therefore, the calculated results predict that the 2-amino-1,4-dione product is favored over 3-amino-1,4-dione product in water. For other solvent calculations, the CPCM derived energy is nearly identical to that of water when using M06-2X/6-31+G(d,p). This may be the problem of the CPCM model.

In order to better understand solvent effects in this aza-michael reaction, the transition structures of both TS1 and TS2 using M06-2X and QM/MM methods in water were studied, CH_2Cl_2, DMSO and CH_3CN. Figure 3.4 indicates for TS1, attacking from 2-C resulted in similar free energy of activation as that of attacking from 3-C, with the energy values of 18.2 kcal/mol and 16.7 kcal/mol, respectively. This is identical to the energy values obtained from *ab initio* calculations (Entry 4, Table 3.1)

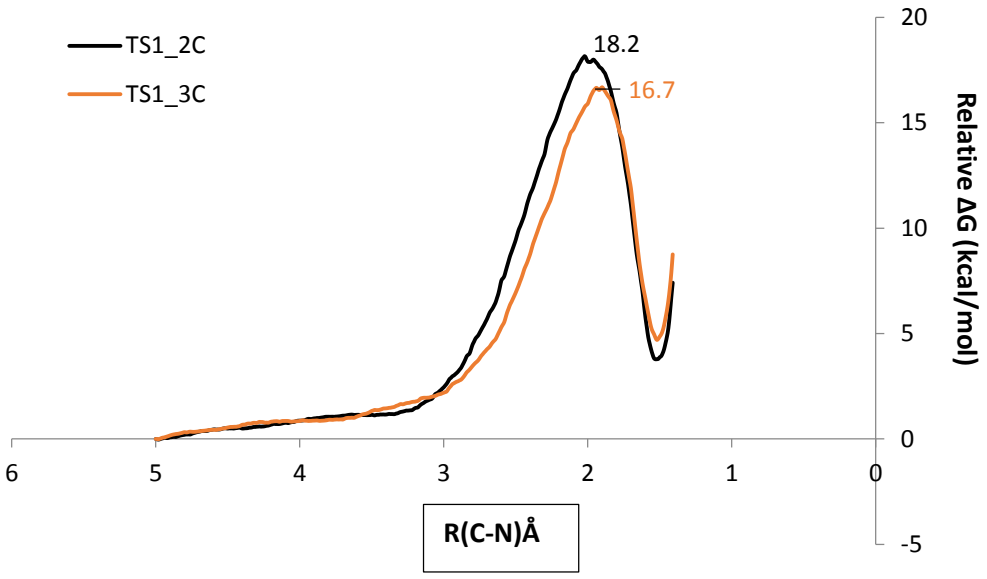

Figure 3.4 QM/MM study of TS1_2C and TS1_3C

For the rate-determining step, TS2 shows different trend when using different solvents. With water, which is polar and protonic, as reaction medium, $\Delta G^{\ddagger}$ of TS2_2C and TS2_3C is 21.0 and 24.0 kcal/mol, respectively (Figure 3.5). The distance between the proton on nitrogen and the 2C or 3C on 1,4-dione was perturbed for QM/MM calculations of TS2_2C and TS2_3C, respectively. This predicts that 2C is the major product in water. When using another polar solvent (CH_3CN), $\Delta G^{\ddagger}$ of TS2_2C is 2 kcal/mol lower than that of TS2_3C.

Since water plays a significant role in assisting hydrogen transfer in the rate-determining step, we want to model this water-assisted proton shuttle using the QM/MM method. A 2D perturbation energy map was constructed using the following approach: the proton shuttle between N and O and another proton shuttle between C and O in Figure 3.3, while the distance of N and O and the distance of C and O was fixed at 2.75 Å (Figure 3.6).

Free energy of activation for the water-assisted proton transfer step of attacking 2C is 23.6 kcal/mol. Figure 3.7 shows a QM/MM simulation water box for TS2 with water-assisted hydrogen transfer. The solute is in the middle.

Table 3.4. Free energy of activation for solvent-assisted hydrogen transfer in various solvents

	$\Delta G^{\ddagger}$(kcal/mol)	
Solvents	TS2_2C	TS2_3C
Water	21.0	24.0
CH_2Cl_2	29.3	30.2
DMSO	25.3	24.4
CH_3CN	24.8	26.9

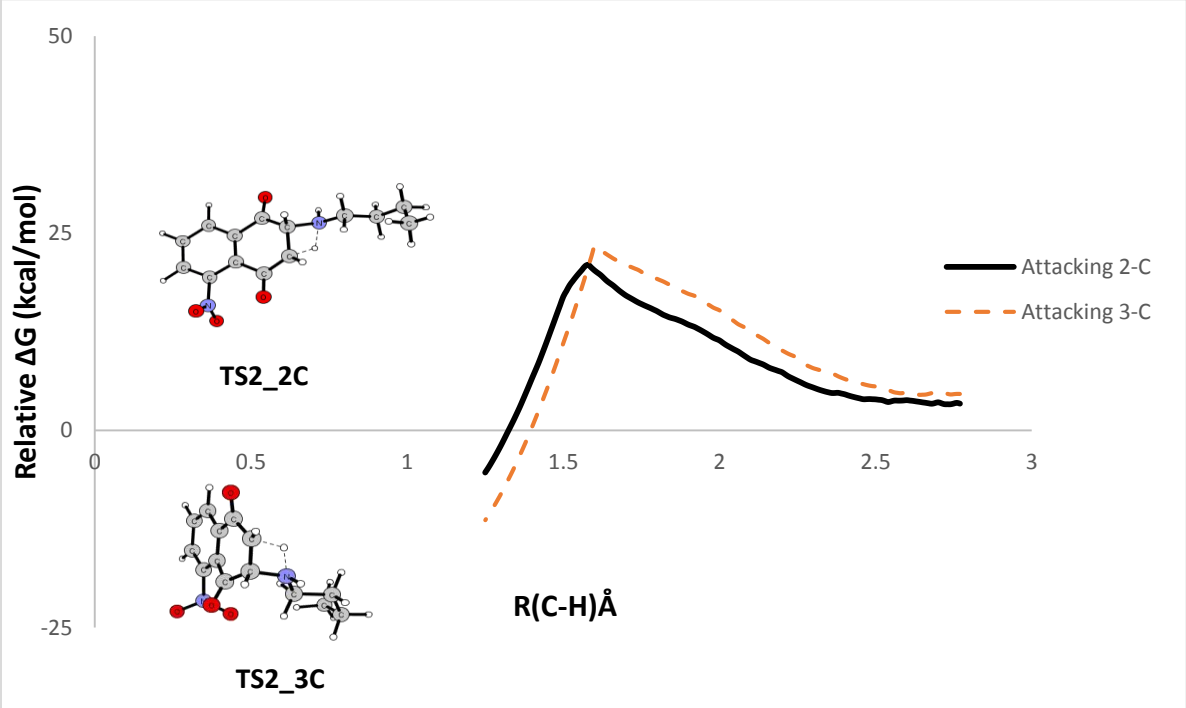

Figure 3.5 Potential energy surface of TS2_2C and TS2_3C under QM/MM

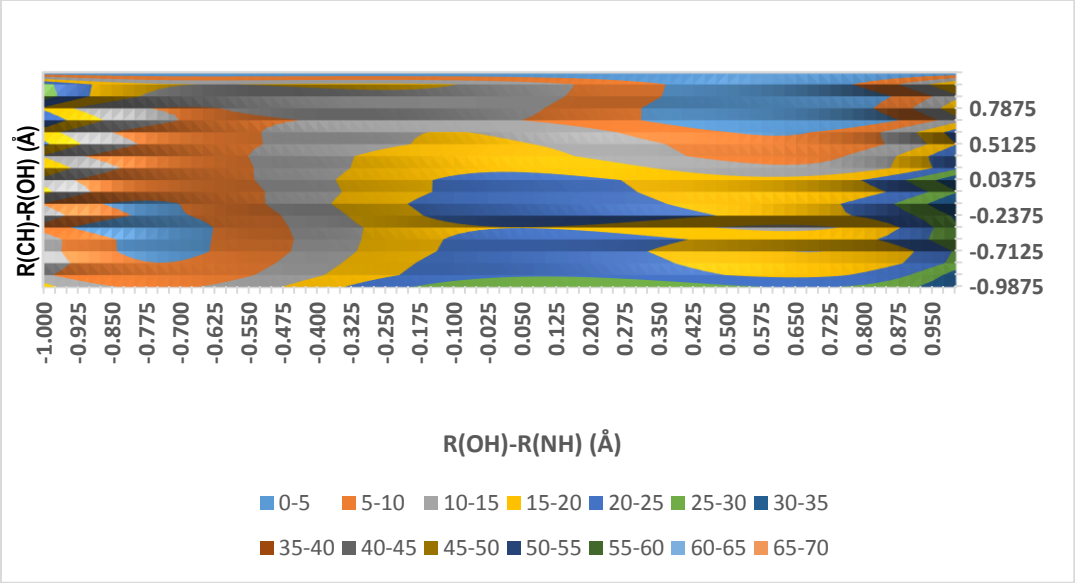

Figure 3.6 2D perturbation energy map of water-assisted hydrogen transfer step using QM/MM for TS2_2C

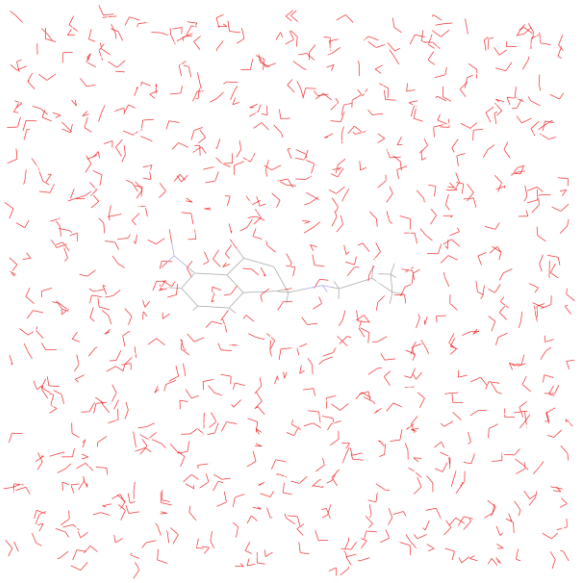

Figure 3.7 QM/MM Simulation Box for TS2_2C with water-assisted hydrogen transfer

3.4 Conclusion

A comprehensive semi-empirical and DFT mechanistic study regarding the mechanism and solvent effects of aza-michael addition has been performed. Among all methods used, M06-2X had the best performance in terms of thermochemistry calculation and hydrogen bonding effects. When using a polar solvent such as water, 2-amino-1,4-dione was obtained as the major product. For transition structure calculations in the intramolecular hydrogen transfer step, a water molecule eases proton transfer from nitrogen of amine to carbon on 1, 4-diketones, reducing the strain of the transition structure dramatically. Because of this water-assisted proton transfer, the activation energy in the intramolecular hydrogen transfer step is much lower than that without water-assisted proton shuffle. For the reaction calculation in water, 2-amino-1,4-dione is the major product which is explained by the stabilization of two H-bonding interactions in the second transition structure.

Chapter 4 Paal-Knorr reaction mechanism study in deep eutectic solvent

4.1 Abstract

In the present work, the Paal-Knorr reaction mechanism of synthesizing furan was explored using both QM and QM/MM methods to gain insight on how solvent influences the mechanism. We started off by looking for the transition structure of pathway b, c and d in Scheme 4.1 using QM methods, followed by a QM/MM/MC calculation for a comparison between a continuum and an explicit solvent model. The mechanism in choline chloride/urea deep eutectic solvent is also proposed to see how solutes interact with the solvents.

4.2 Computational Methods

Reactants and transition states were located in 725 explicit water molecules represented using the TIP4P water model[74] and the OPLS-AA force field for non-aqueous solutions.[75,76] The solutes were treated using the PDDG/PM3 semi-empirical QM method,[77] which has been reported to give very good results for a wide variety of organic and enzymatic reactions in the solution phase.[78] Calculations of atomic charges and QM energy are performed for each attempted move of the solute, which happens every 100 configurations. CM3 charges[79] were obtained for the solute with a scaling factor of 1.14 for electrostatic contributions to the solute-solvent energy. Lennard-Jones interactions between solvent and solute atoms were taken into account using OPLS parameters. This combination minimizes errors in the computed free energies of hydration for a PM3-based method.[80] Free energy changes were calculated using free energy perturbation (FEP) theory in conjunction with isothermal-isobaric (NPT) Metropolis Monte Carlo simulations at

25 °C and 1 atm. The starting geometry of solute was determined by the PDDG/PM3 method. Each FEP calculation entailed ca. 10 million configurations of equilibration and 20 million configurations of averaging at the increments of 0.01Å for the making/breaking bond distances. Double wide sampling was used to increase computing efficiency.

The BOSS program was used to conduct all QM/MM reactions from the stored and custom-made solvent boxes.[81] All solvents were fully flexible, with the exception of water, which already exists in BOSS as a fixed united-atom solvent. Periodic boundary conditions have been applied to tetragonal boxes containing 725 water molecules. Solute-solvent and solvent-solvent cutoffs of 12 Å were used with quadratic feathering of the intermolecular interactions with 0.5 Å of the cutoff. The BOSS program sets the ranges for bond stretching and angle bending automatically on the basis of force constants and temperature. All QM/MM/MC calculations were run on Alabama Supercomputer Center.

For comparison, the M06-2X density functional method and the 6-31+G(d,p) basis set were also used to optimize geometries in water using Gaussian 09.[83] The effect of solvent was explored by full DFT geometry optimizations using the SMD solvation model.[97] Frequency calculations were performed in order to verify all stationary points as minima for ground states or as saddle points for transition structures. All calculations were run on computers located at the Alabama Supercomputer Center.

4.3 Results and Discussion

In the Paal-Knorr reaction under choline chloride/urea, it has been proposed that the carbonyl group is activated by a hydrogen-bonding interaction between the carbonyl oxygen and hydrogens on urea (Figure 4.1), followed by a nucleophilic attack of the

adjacent carbonyl oxygen to the carbonyl carbon and then a completion of the cyclization step.[58]

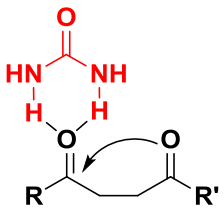

Figure 4.1 Hydrogen-bonding interaction between urea and diketone reactant

An initial model (Figure 4.2) was employed to provide preliminary data on the transition structure along different reaction pathways. In this model, a proton is employed to activate the carbonyl group, making it more electrophilic.

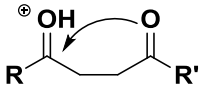

Figure 4.2 Paal-Knorr reaction with an activated carbonyl group

With this simplified model as the starting point, the transition structures of pathway b and d (Scheme 4.1) were located successfully using the M06-2X/6-31+G(d,p) method with the SMD solvation model for water. For pathway d which is a nucleophilic attack of one carbonyl oxygen to the other protonated carbonyl followed by rapid proton removal, two transition structures along with the reaction intermediate were located (Figure 4.4, Figure 4.5, Figure 4.5).

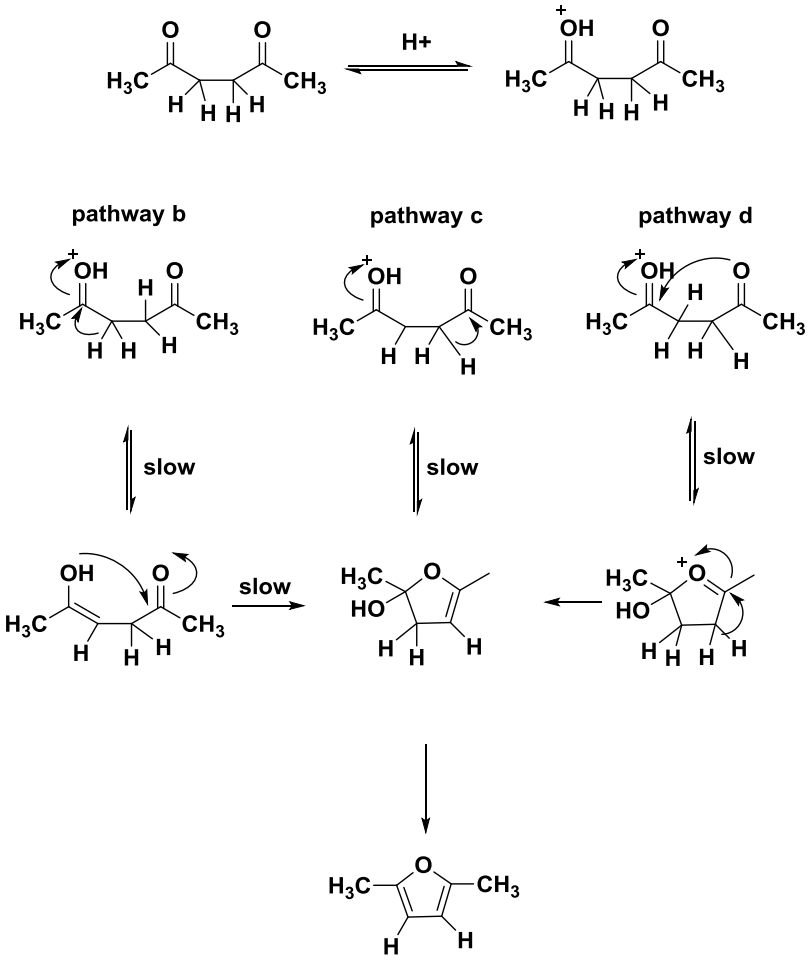

Scheme 4.1 Proposed Paal-Knorr mechanisms[61]

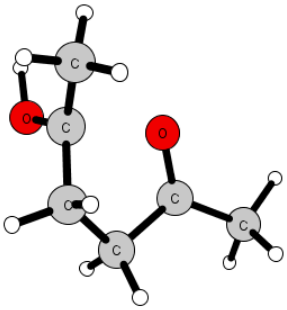

Figure 4.3 Transition structure of the nucleophilic attack step of pathway d (TS1)

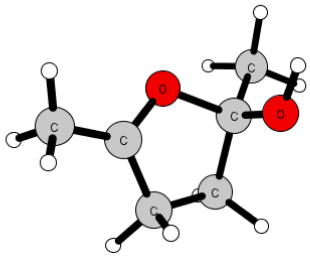

Figure 4.4 Calculated reaction intermediate after the nucleophilic attack step of pathway d

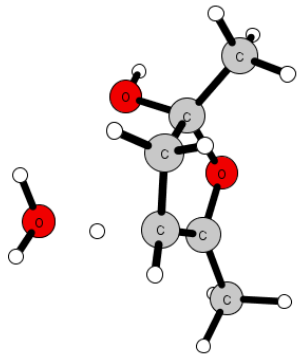

Figure 4.5 Transition structure of the proton removal by water in pathway d (TS2)

For pathway d, free energy of activation for TS1 and TS2 is -1.0 kcal/mol and 9.1 kcal/mol, respectively. The reason why TS2 has much higher activation energy is probably because water molecule is employed to abstract the proton.

The transition structure of the nucleophilic attack step of pathway d was also found using the QM/MM/MC calculation in a water box containing 725 water molecules (Figure

4.5). The potential energy surface for simulation of this step is shown in Figure 4.7. The C-O bond was mutated from 3.0 Å to 1.4 Å at the increment of 0.1 Å. At 3.0 Å, the structure is the protonated 1,4-dione. The transition structure found is similar to the geometry from the M062X/6-31+G(d,p) method.

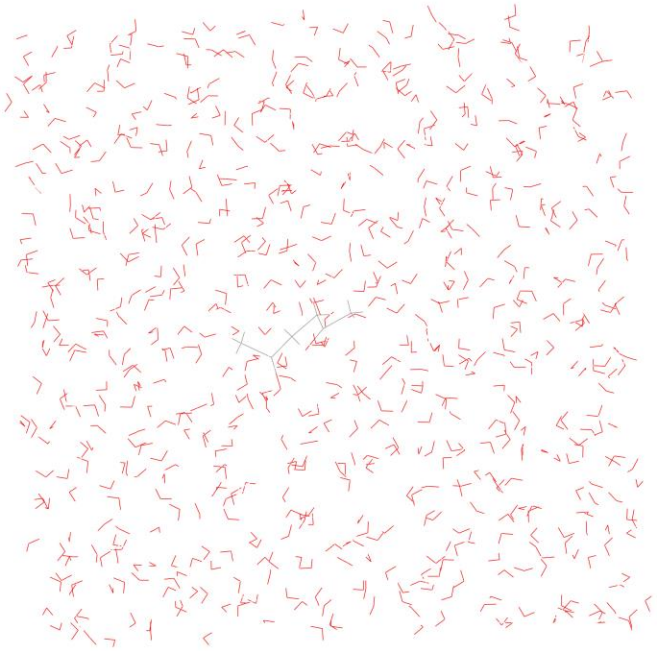

Figure 4.6 QM/MM simulation box for the Paal-Knorr reaction

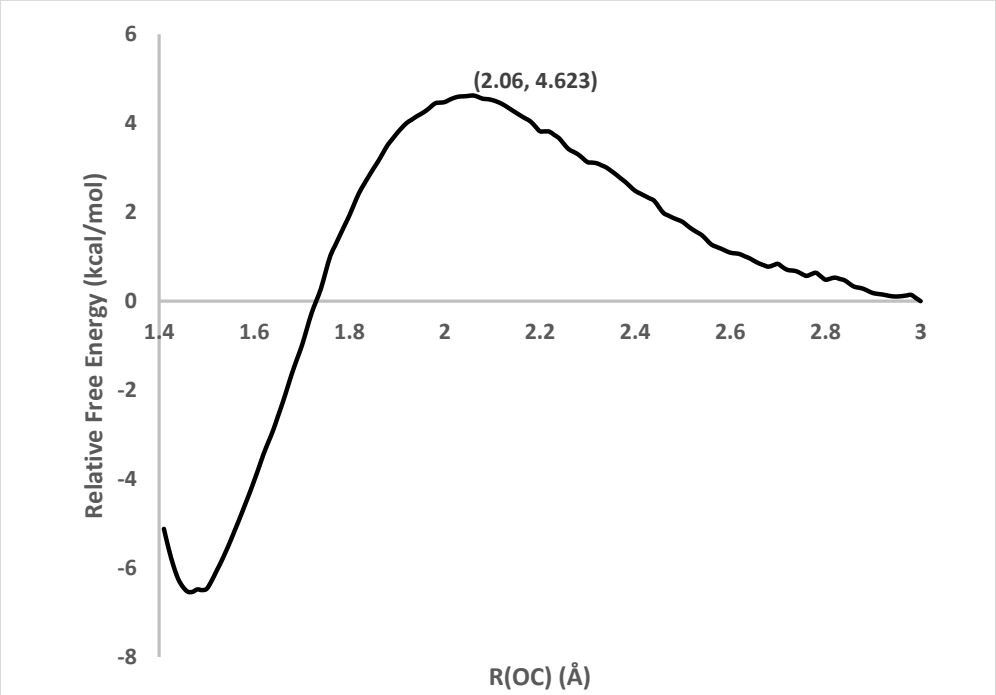

Figure 4.7 Free energy curve of the QM/MM simulation of the nucleophilic attack step in pathway d for the Paal-Knorr reaction

The distance between the carbonyl oxygen and the activated carbonyl carbon was 2.06 Å, compared to 1.99 Å to that of M06-2X method. Significant effort was put on pathway b to try to find the associated transition structure. However, no transition structure was located. Instead, when the carbonyl oxygen on the fifth carbon was protonated, the expected TS is found (Figure 4.8). This indicated that a more activated carbonyl group is needed to lower the activation barrier for the nucleophilic attack of oxygen to carbonyl carbon.

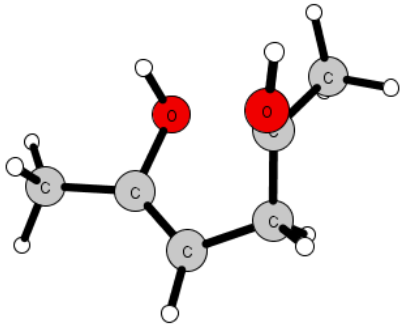

Figure 4.8 Transition state structure of the nucleophilic attacking step of pathway b with the protonated carbonyl group in the Paal-Knorr reaction

For pathway c which is the concerted proton removal and cyclization to ring closure product, water and methanol were used for proton removal during the calculation. Unfortunately, we were unable to locate any transition structure of the favored pathway c discussed previously. The possible reason is that this concerted pathway requires very high activation energy.

4.4 Conclusion

A preliminary DFT and QM/MM study was performed to gain insight on the mechanism of the Paal-Knorr synthesis of furan. This reaction was proposed previously to have three different pathways which are proton removal first and then cyclization (pathway b), cyclization and then proton removal (pathway d) and the concerted pathway (pathway c). For pathway d, transition structures of both cyclization and proton abstraction step are located using the M06-2X method with the 6-31+G(d,p) basis set and the SMD solvation

model for water. The QM/MM study predicts a similar transition structure as that of M06-2X. Future work will be first focused on the transition structures calculation of pathway b and pathway c for Paal-Knorr reaction using a protonic acid or urea as catalyst. Next we will perform the QM/MM calculations to gain insight on how the reactants interact with the CC/U solvent and how the eutectic solvent influences the reaction mechanism. Then we want to explore the solvent effects and reaction mechanism for other eutectic solvents such as CC/G.

References

(1) Shibasaki, M.; Sasai, H.; Arai, T. *Angew. Chem. Int. Ed. Engl.* **1997**, *36*, 1236-1256.

(2) Gellman, S. *Acc. Chem. Res.* **1998**, *31*, 173-180.

(3) Bartoli, G.; Cimarelli, C.; Marcantoni, E.; Palmieri, G.; Petrini, M. *J. Org. Chem.* **1994**, *59*, 5328-5335.

(4) Cardillo, G.; Tomasini, C. *Chem. Soc. Rev.* **1996**, *25*, 117-128.

(5) Hayashi, Y.; Rode, J. J.; Corey, E. *J. Am. Chem. Soc.* **1996**, *118*, 5502-5503.

(6) Arend, M.; Westermann, B.; Risch, N. *Angew. Chem. Int. Ed. Engl.* **1998**, *37*, 1044-1070.

(7) Sokoloff, N.; Latschinoff, P. *Ber. Dtsch. Chem. Ges.* **1874**, *7*, 1384-1387.

(8) Heintz, W.; Sokoloff, N.; Latschinoff, P. *Ber. Dtsch. Chem. Ges.* **1874**, *7*, 1518-1520.

(9) Haeseler, P. R. *Org. Synth.* **1926**, *6*, 28-30.

(10) Bull, S. D.; Davies, S. G.; Delgado-Ballester, S.; Fenton, G.; Kelly, P. M.; Smith, A. D. *Synlett* **2000**, *2000*, 1257-1260.

(11) Davies, S. G.; McCarthy, T. D. *Synlett* **1995**, 700-702.

(12) Giuseppone, N.; Vander Weghe, P.; Mellah, M.; Collin, J. *Tetrahedron* **1998**, *54*, 13129-13148.

(13) Sibi, M. P.; Liu, M. *Org. Lett.* **2000**, *2*, 3393-3396.

(14) Zhuang, W.; Hazell, R. G.; Jorgensen, K. A. *Chem. Commun.* **2001**, 1240-1241.

(15) Tian, S.; Arredondo, V. M.; Stern, C. L.; Marks, T. J. *Organometallics* **1999**, *18*. 2568-2570.

(16) Arredondo, V. M.; Tian, S.; McDonald, F. E.; Marks, T. J. *J. Am. Chem. Soc.* **1999**, *121*, 3633-3639.

(17) Beller, M.; Trauthwein, H.; Eichberger, M.; Breindl, C.; Herwig, J.; Muller, T. E. *Chem. Eur. J.* **1999**, *5*, 1306-1319.

(18) Bandgar, B. P.; Kasture, S. P. *Green Chem.* **2000**, *2*, 154-156.

(19) Ponde, D. E.; Deshpande, V. H.; Bulbule, V. J.; Sudalai, A.; Gajare, A. S. *J. Org. Chem.* **1998**, *63*, 1058-1063.

(20) Kawatsura, M.; Hartwig, J. F. *Organometallics* **2001**, *20*, 1960-1964.

(21) Loh, T. P.; Wei, L. L. *Synlett* **1998**, 975-976.

(22) Xu, L. W.; Li, L.; Xia, C. G. *Helv. Chim. Acta* **2004**, *87*, 1522-1526.

(23) Narayan, S.; Muldoon, J.; Finn, M. G.; Fokin, V. V.; Kolb, H. C.; Sharpless, K. B. *Angew. Chem. Int. Ed.* **2005**, *44*, 3275-3279.

(24) Butler, R. N.; Coyne, A. G. *Chem. Rev.* **2010**, *110*, 6302-6337.

(25) Carlone, A.; Marigo, M.; North, C.; Landa, A.; Jorgensen, K. A. *Chem. Commun.* **2006**, 4928-4930.

(26) Cao, Y. J.; Lai, Y. Y.; Wang, X.; Li, Y. H.; Xiao, W. J. *Tetrahedron Lett.* **2007**, *48*, 21-24.

(27) Phippen, C. B. W.; Beattie, J. K.; McErlean, C. S. P. *Chem. Commun.* **2010**, *46*, 8234-8236.

(28) Hallett, J. P.; Welton, T. *Chem. Rev.* **2001**, *111*, 3508-3576.

(29) Welton, T. *Chem. Rev.* **1999**, *99*, 2071-2083.

(30) Hohenberg, P. *Phys. Rev.* **1964**, *136*, B86–B871.

(31) MacFarlane, D. R.; Pringle, J. M.; Johansson, K. M.; Forsyth, S. A.; Forsyth, M. *Chem. Commun.* **2006**, 1905.

(32) Davis, J. H. *Chem. Lett.* **2004**, *33*, 1072.

(33) Dupont, J.; de Souza, R. F.; Suarez, P. A. Z. *Chem. Rev.* **2002**, *102*, 3667.

(34) Valkenberg, M. H.; deCastro, C.; Ho¨lderich, W. F. *Green Chem.* **2002**, *4*, 88.

(35) Zhao, D.; Fei, Z.; Geldbach, T. J.; Scopelliti, R.; Dyson, P. J. *J. Am. Chem. Soc.* **2004**, *126*, 15876.

(36) Allen, C.; Sambasivarao, S. V.; Acevedo, O. *J. Am. Chem. Soc.* **2013**, *135*, 1065-1072.

(37) D'Anna, M. M.; Gallo, V.; Mastrorilli, P.; Nobile, C. F.; Romanazzi, G.; Suranna, G. P. *Chem. Commun.* **2002**, 434.

(38) Yadav, J. S.; Reddy, B. V. S.; Baishya, G.; Narsaiah, A. V. *Chem. Lett.* **2005**, *34*, 102.

(39) Gallo, V.; Giardina-Papa, D.; Mastrorilli, P.; Nobile, C. F.; Suranna, G. P.; Wang, Y. *J. Organomet. Chem.* **2005**, *690*, 3535.

(40) Wang, Z.; Wang, Q.; Zhang, Y.; Bao, W. *Tetrahedron Lett.* **2005**, *46*, 4657.

(41) Xu, L. W.; Li, J. W.; Zhou, S. L.; Xia, C. G. *New J. Chem.* **2004**, *28*, 183.

(42) Xu, L. W.; Li, L.; Xia, C. G.; Zhou, S. L.; Li, J. W. *Tetrahedron* **2004**, *45*, 1219.

(43) Kantam, M. L.; Neeraja, V.; Kavita, B.; Neelima, B.; Chaudhuri, M. K.; Hussain, S. *AdV. Synth. Catal.* **2005**, *347*, 763.

(44) Trost, B. M.; Doherty, G. A. *J. Am. Chem. Soc.* **2000**, *122*, 3801-3810.

(45) Fürstner, A.; Szillat, H.; Gabor, B.; Mynott, R. *J. Am. Chem. Soc.* **1998**, *120*, 8305-8314.

(46) Rahmatpour, A.; Aalaie, J. *Heteroatom Chem.* **2011**, *22*, 85-90.

(47) Noronha, R. G. d.; Fernandes, A. C.; Romão, C. C. *Tetrahedron Lett.* **2009**, *50*, 1407-1410.

(48) Leadbeater, N. E.; Marco, M. *Chem. Rev.* **2002**, *102*, 3217-3274.

(49) Plechkova, N. V.; Seddon K. R. *Chem. Soc. Rev.* **2008**, *37*, 123-150.

(50) Abbott, A. P.; Boothby, D.; Capper, G.; Davies, D. L.; Rasheed, R. K. *J. Am. Chem. Soc.* **2004**, *126*, 9142-9147.

(51) Zhang, Q.; De Oliveira Vigier, K.; Royer, S.; Jerome, F. *Chem. Soc. Rev.* **2012**, *41*, 7108-7146.

(52) Abbott, A. P.; Capper, G.; Davies, D. L.; Rasheed, R. K.; Tambyrajah, V. *Chem. Comm.* **2003**, 70-71.

(53) D'Agostino, C.; Harris, R. C.; Abbott, A. P.; Gladden, L. F.; Mantle, M. D. *Phys. Chem. Chem. Phys.* **2011**, *13*, 21383-21391.

(54) Ilgen, F.; Ott, D.; Kralisch, D.; Reil, C.; Palmberger, A.; Konig, B. *Green Chem.* **2009**, *11*, 1948-1954.

(55) Stolte, S.; Abdulkarim, S.; Arning, J.; Blomeyer-Nienstedt, A.-K.; Bottin-Weber, U.; Matzke, M.; Ranke, J.; Jastorff, B.; Thoming, J. *Green Chem.* **2008**, *10*, 214-224.

(56) Garcia-Alvarez, J.; Diez, J.; Gimeno, J. *Green Chem.* **2010**, *12*, 2127-2130.

(57) Imperato, G.; Hoger, S.; Lenoir, D.; Konig, B. *Green Chem.* **2006**, *8*, 1051-1055.

(58) Handy, S.; Lavender, K. *Tetrahedron Lett.* **2013**, *54*, 4377-4379.

(59) Szakal-Quin, G.; Graham, D. G.; Millington, D. S.; Maltby, D. A.; McPhail, A. T. *J. Org. Chem.* **1986**, *51*, 621-624.

(60) Amarnath, V.; Anthony, D. C.; Amarnath, K.; Valentine, W. M.; Wetterau, L. A.; Graham, D. G. *J. Org. Chem.* **1991**, *56*, 6924-6931.

(61) Amarnath, V.; Amarnath, K. *J. Org. Chem.* **1995**, *60*, 301-307.

(62) Shelly, K. P.; Venimadhavan, S.; Nagarajan, K.; Stewart, R. *Can. J. Chem.* **1989**, *67*, 1274-1282.

(63) Leach, A. R. *Molecular Modelling: Principles and Applications*; 2nd ed.; Pearson Education Limited: Essex, 2001.

(64) Hehre, W. J. *A Guide to Molecular Mechanics and Quantum Chemical Calculations*; Wavefunction Inc: Irvine, 2003.

(65) Szabo, A.; Ostlund, N. S. *Modern Quantum Chemistry: Introduction to Advanced Electronic Structure Theory*; Dover Publications, Inc: New York, 1996.

(66) Kohn, W.; Sham, L. J. *Phys. Rev.* **1965**, *140*, A1133-A1138.

(67) Zhao, Y.; Truhlar, D. G. *Acc. Chem. Res.* **2008**, *41*, 157-167.

(68) Cramer, C. J. Essentials of Computational Chemistry; 2nd ed ed.; John Wiley and Sons Ltd.: West Sussex, England, 2004.

(69) Raghavachari, K.; Trucks, G. W.; Pople, J. A.; Head-Gordon, M. *Chem. Phys. Lett*. **1989**, *157*, 479-483.

(70) Jorgensen, W. L.; Maxwell, D. S.; Tirado-Rives, J. *J. Am. Chem. Soc.* **1996**, *118*, 11225-11236.

(71) Jorgensen, W. L.; Madura, J. D.; Swenson, C. J. *J. Am. Chem. Soc.* **1984**, *106*, 6638-6646.

(72) Jorgensen, W. L.; Tirado-Rives, J. *J. Am. Chem. Soc.* **1988**, *110*, 1657-1666.

(73) Winget, P.; Thompson, J. D.; Xidos, J. D.; Cramer, C. J.; Truhlar, D. G. *J. Phys. Chem. A* **2002**, *106*, 10707-10717.

(74) Jorgensen, W. L.; Chandrasekhar, J.; Madura, J. D.; Impey, W.; Klein, M. L. *J. Chem. Phys*. **1983**, *79*, 926-935.

(75) Jorgensen, W. L.; Tirado-Rives, J. *Proc. Natl. Acad. Sci*. **2005**, *102*, 6665–6670.

(76) Jorgensen, W. L.; Maxwell, D. S.; Tirado-Rives, J. *J. Am. Chem. Soc*. **1996**, *118*, 11225-11236.

(77) Tubert-Brohman, I.; Guimara˜es, C. R. W.; Jorgensen, W. L. *J. Chem. Theory Comput*. **2005**, *1*, 817-823.

(78) Acevedo, O.; Jorgensen, W. L. *Acc. Chem. Res*. **2010**, *43*, 142-151.

(79) Thompson, J. D.; Cramer, C. J.; Truhlar, D. G. *J. Comput. Chem*. **2003**, *24*, 1291-1304.

(80) Blagovic´, M. U.; Morales de Tirado, P.; Pearlman, S. A.; Jorgensen, W. L. *J. Comput. Chem*. **2004**, *25*, 1322-1332.

(81) Jorgensen, W. L.; Tirado-Rives, J. *J. Comput. Chem*. **2005**, *26*, 1689-1700.

(82) Jorgensen, W. L. *J. Phys. Chem*. **1986**, *90*, 1276-1284.

(83) Frisch, M. J.; Trucks, G. W.; Schlegel, H. B.; Robb, M.; Cheeseman, J. R.; Scalmani, G.; Barone, V.; Petersson, G. A.; Nakatsuji, H.; Caricato, M.; Li, X.; Izmaylov, A. F.; Bloino, J.; Zheng, G.; Sonnenberg, J. L.; Ehara, M.; Toyota, K.; Fukuda, R.; Hasegawa, J.; Ishida, M.; Honda, Y.; Kitao, O.; Nakai, H.; Vreven, T.; Peralta, J. E.; Ogliaro, F.; Bearpark, M.; Heyd, J. J.; Kudin, K. N.; Staroverov, V. N.; Keith, T.; Kobayashi, R.; Raghavachari, K.; Rendell, A.; Burant, J. C.; Iyengar, S. S.; Cossi, M.; Rega, N.; Millam, J. M.; Klene, M.; Knox, J. E.; Bakken, V.; Adamo, C.; Jaramillo, J.; Gomperts, R.; Yazyev, O.; Austin, A. J.; Cammi, R.; Pomelli, C.; Martin, R. L.; Morokuma, K.; Zakrzewski, V. G.; Salvador, P.; Dannenberg, J. J.; Dapprich, S.; Farkas, O.; Foresman, J. B.; Ortiz, J. V.; Fox, D. Gaussian 09, Revision B.01; Gaussian, Inc.: Wallingford, CT, 2010.

(84) Tomasi, J.; Mennucci, B.; Cammi, R. *Chem. Rev*. **2005**, *105*, 2999-3093.

(85) Repasky, M. P.; Chandrasekhar, J.; Jorgensen, W. L. *J. Comput. Chem*. **2002**, *23*, 1601-1622.

(86) Korth, M.; Pitonak, M.; Rezac, J.; Hobza, P. *J. Chem. Theory Comput*. **2010**, *6*, 334-352.

(87) Rezac, J.; Hobza, P. *J. Chem. Theory Comput*. **2012**, *8*, 141-151.

(88) Fustero, S.; Chiva, G.; Piera, J.; Volonterio, A.; Zanda, M.; Gonzalez, J.; Ramallal, A. M. *Chem. Eur. J.* **2007**, *13*, 8530-8542.

(89) Schreiner, P. R. *Angew. Chem. Int. Ed*. **2007**, *46*, 4217-4219.

(90) Woodcock, H. L.; Schaefer III, H. F.; Schreiner, P. R. *J. Phys, Chem. A* **2002**, *106*, 11923-11931.

(91) Grimme, S. *J. Chem. Phys.* **2003**, *118*, 9095-9102.

(92) Zhao, Y.; Schultz, N. E.; Truhlar, D. G. *J. Chem. Theory Comput*. **2006**, *2*, 364-382.

(93) Okumoto, S. *J. Org. Chem*. **2000**, *65*, 1544-1548.

(94) Xia, Y. Z.; Liang, Y.; Y., C. Y.; Wang, M.; L., J.; Huang, F.; Liu, S.; Li, Y. H.; Yu, Z. X. *J. Am. Chem. Soc.* **2007**, *129*, 3470-3471.

(95) Shi, F. Q.; Li, X.; Xia, Y. Z.; Zhang, L. M.; Yu, Z. X. *J. Am. Chem. Soc*. **2007**, *129*, 15503-15512.

(96) Marenich, A. V.; Cramer, C. J.; Truhlar, D. G. *J. Phys, Chem. B* **2009**, *113*, 6378-6396.